American Mineralogist, Volume 66, pages 908-930, 1981

Petrology of graphitic sulfide-rich schists from south-central Maine: an example of desulfidation during prograde regional metamorphism

JOHN M. FERRY

Department of Geology
Arizona State University
Tempe, Arizona 85281

Abstract

Graphitic sulfide-rich schists from a Buchan-type metamorphic terrain contain assemblages of silicate, sulfide, oxide, and carbonate minerals metamorphosed from chlorite through sillimanite zone conditions. Sulfidic marine black shales, the protoliths of the graphitic sulfide-rich schists, contain pyrite but either only traces of pyrrhotite or no pyrrhotite at all. The appearance of abundant pyrrhotite in the graphitic sulfide-rich schists, therefore, documents the conversion of pyrite to pyrrhotite during metamorphism. Mineralogical, mineral chemical, and whole-rock chemical data for the sulfide-rich schists indicate that the pyrite → pyrrhotite transition occurs by desulfidation at constant whole-rock iron contents without participation of silicate minerals. The metamorphic reaction that converts pyrite to pyrrhotite is unusual in two respects: (a) products and reactants are quenched in at least some specimens in all metamorphic zones studied and (b) the reaction has gone to completion in some samples from each metamorphic zone. Increasing temperature (grade) is thus unlikely to exercise a dominant control over the reaction. Consideration of the amounts of iron sulfides in the schists and the composition of C–O–H–S fluids with which the rocks were in equilibrium leads to the conclusion that enormous volumes of fluid flushed through the schists during the metamorphic event (volumetric fluid-rock ratios > 1). The flow of large volumes of fluid through the schists serves as a mechanism that drives the desulfidation reaction.

Introduction

Iron sulfides, pyrite and pyrrhotite, are constituents of many pelitic schists, and the sulfides react both with each other and with other phases in schists during prograde metamorphism. Carpenter (1974), for example, mapped an isograd based on the conversion of pyrite to pyrrhotite in pelitic schists from Tennessee and North Carolina. Robinson and Tracy (1976) and Guidotti *et al.* (1976) found systematic relationships between the compositions of Fe–Mg minerals and the identity of coexisting iron sulfides in schists from Massachusetts and Maine, respectively. Guidotti (1970a) used sulfide–silicate equilibria to estimate the composition of fluid in equilibrium with pelitic rocks during metamorphism. In spite of the common occurrence of iron sulfides in schists, there is little detailed knowledge of the mineral reactions in which pyrite and pyrrhotite participate over a wide range of metamorphic grades. This report presents mineralogical and chemical data for a suite of graphitic sulfide-rich schists from chlorite through sillimanite grades. The first goal of the report is to examine mineral equilibria in these rocks as a function of grade and, specifically, (1) to determine whether the commonly observed pyrite–pyrrhotite transition may be mapped as an isograd; (2) to determine the mineral reaction that is associated with the pyrite–pyrrhotite transition; and (3) to determine whether any other reactions involving iron sulfides occur with prograde metamorphism.

A second goal of this report is to use mineralogical and chemical data from the graphitic sulfide-rich schists to evaluate whether significant mass transport of sulfur occurs during prograde metamorphism. Mass transfer of sulfur during metamorphism is a contentious issue. Some have found evidence for transport of sulfur around metamorphosed sulfide deposits (Fullagar *et al.*, 1967; Popp, 1977), while others have argued that mass transfer of sulfur does not normally occur during metamorphic events (Thompson, 1972; Robinson *et al.*, 1976). Iron sul-

0003–004X/81/0910–0908$02.00

fides are the principal repository for sulfur in pelitic schists. Consequently the petrologic behavior of sulfides is important because they are the main clue for elucidation of whether mass transport of sulfur occurs during metamorphism.

Geological setting

Samples were collected from the Silurian Waterville and Sangerville Formations in south-central Maine (Fig. 1). Samples from the Sangerville Formation were collected within 100 m of its contact with the Waterville Formation. The formations are composed of interbedded shale, argillaceous limestone, and argillaceous sandstone and their metamorphic equivalents. Compositional layering is on a scale of 1–8 cm. Most samples of graphitic sulfide-rich schist were collected from discontinuous but mappable horizons. Three samples (196A, 711B, 919G) were collected from graphitic sulfide-rich beds in outcrops of otherwise normal pelitic schist. The three samples are not unusual in composition relative to samples collected from mappable horizons of graphitic sulfide-rich schist.

The area in Figure 1 is a Buchan-type metamorphic terrain, and Osberg (personal communication, 1976) has mapped isograds in the Waterville Formation based on the first appearance of biotite, garnet, staurolite + andalusite, and sillimanite in pelitic schists. Metasediments are folded into isoclinally refolded recumbant folds (Osberg, 1979) and are intruded by two-mica quartz monzonite stocks. Porphyroblasts of garnet, staurolite, andalusite, cordierite, and sillimanite cut across schistosity associated with the isoclinal folds in the area. The peak of regional metamorphism followed almost all the deformation. Ferry (1978) has argued that metamorphism and intrusion of the granitic rocks were at least broadly synchronous. Geochronologic work on both the granitic and metamorphic rocks indicates that the metamorphism and granite emplacement occurred during the Devonian Acadian Orogeny (Dallmeyer, 1979). Evidence for three metamorphic episodes (one well to the west of the present area) has been reported for rocks of the western part of the Augusta Quadrangle by Novak and Holdaway (1981). They suggest that low-variance assemblages and limited textural evidence of disequilibrium imply presence of two metamorphic episodes (possibly M_2 and M_3 of Guidotti, 1970b) in the area immediately west of the present map area. If there were two metamorphic events in the present area, they were closely-spaced in time and P–T conditions and the rocks in question appear to have entirely equilibrated to the last and most pervasive event (possibly M_3).

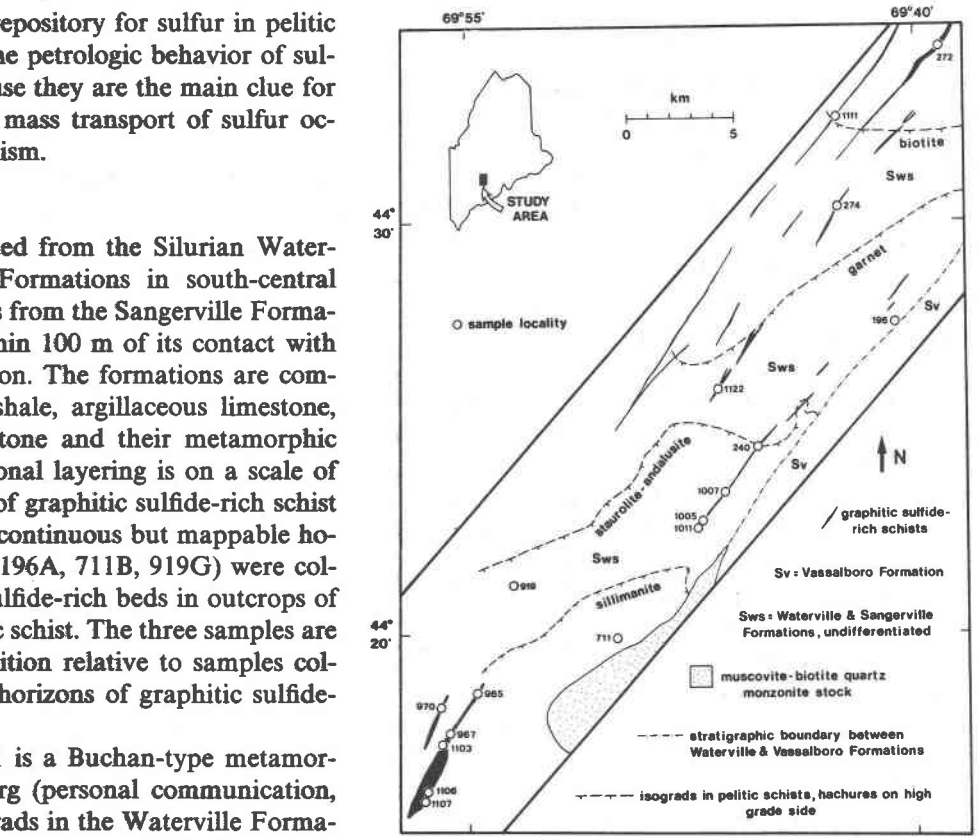

Fig. 1. Geologic sketch map of study area. Data from Osberg (1968; personal communication); Barker (1964); Ferry (1978).

Pressure and temperature

Estimates of pressure and temperature attained during metamorphism in the study area are summarized by Ferry (1980b). Pressure was 3500±200 bars near the sillimanite isograd. Temperatures ranged from ~ 375°C at the biotite isograd to 550°–575°C in the sillimanite zone. Mean temperatures for the metamorphic zones in Figure 1, based on the biotite–garnet Fe–Mg exchange geothermometer, are: garnet zone, 460°C; staurolite + andalusite zone, 490°C; sillimanite zone, 550°C.

Methods of investigation

Nineteen samples of graphitic sulfide-rich schists were collected. Sulfide-rich schists were differentiated from normal pelitic schists by their greater sulfur content (arbitrarily taken as > 1 weight percent sulfur). The locations of samples used in the report are given in Figure 1.

Thin sections were prepared from rock specimens that correspond in outcrop to individual beds of graphitic sulfide-rich schist. At some outcrops more than one bed was sampled. Most samples appear homogeneous in hand specimen. A few specimens contain sulfide-rich laminations with spacings of approximately 2–5 mm. Thin sections, prepared from slices that cut across the laminations, were sufficiently large to sample a statistically homogeneous volume of laminated rock. Mineral assemblages were identified petrographically using transmitted and reflected light. It was arbitrarily assumed that a group of minerals in the same 2 mm diameter circular domain of a thin section were in equilibrium. Obvious cases of textural disequilibrium such as inclusions of one mineral in another or mantling of one mineral by an aggregate of another were exceptions to this assumption.

Compositions of minerals were obtained with an automated MAC electron microprobe at the Geophysical Laboratory, Carnegie Institution of Washington. Data for silicates were reduced by the method of Bence and Albee (1968) with correction factors by Albee and Ray (1970). Data for sulfides and carbonates were reduced using the MAGIC IV computer program, a ZAF correction scheme (Colby, 1971).

Modal amounts of selected minerals were determined by counting 2000–4000 points in thin section. In general, modal analysis of sulfides in reflected light posed no problems. Products of surficial weathering, limonite and marcasite, were counted as fresh pyrite or pyrrhotite according to the kind of sulfide that it was associated with. Sample 240A contains a substantial amount of secondary marcasite. The marcasite was counted as pyrite and pyrrhotite in the proportions in which fresh pyrite and pyrrhotite occur in the rock. Modal analysis of most silicates was hampered in all samples except those from the sillimanite zone by the fine grain size of the rocks and by finely divided graphitic material. The ubiquitous graphitic material tends to obscure all silicates except biotite. Volume amounts of minerals were converted to molar amounts (per reference volume of rock) using molar volume data (Robie *et al.*, 1967; Hewitt and Wones, 1975).

Chemical analyses of rock samples for major element metal oxides were performed using inductively coupled argon plasma methods by Technical Service Laboratories, Mississauga, Ontario (A. Debnam, analyst). Samples for chemical analysis, approximately 5 cm^3 in volume, were cut from hand specimens as close as possible to where chips were removed to prepare thin sections. Table 1 lists analyses of a Mount Hood andesite which is used as a secondary standard in the XRF laboratory in the Department of Chemistry at Arizona State University. Reliability of the analyses may be assessed by comparing the composition of the Mount Hood andesite with the analysis of the same material performed by Technical Service Laboratories. Whole-rock samples were analyzed for sulfur by Technical Service Laboratories. Samples were fused at over 1800°C in a LECO combustion furnace. During fusion all sulfur was evolved as SO_2 gas. The amount of sulfur was measured by a volumetric titration of the SO_2 gas. Whole-rock samples were also analyzed for total carbon and sulfur by C. F. Lewis in the laboratory of C. B. Moore at Arizona State University. Analytical methods used for sulfur at A.S.U. are those of Moore *et al.* (1972). For the determination of carbon, samples were combusted in a flowing oxygen atmosphere in an induction furnace at over 1800°C to form CO_2. After purification of the effluent gases, the amount of CO_2 was measured using a LECO 762-000 carbon analyzer with an infrared detection system.

Mineralogy and mineral chemistry

The mineralogy of all samples and selected compositional parameters for minerals are compiled in Table 2. Table 3 presents modal proportions of sulfides in all samples and of biotite in selected samples.

Sulfides

All samples contain pyrrhotite which occurs as elongated anhedral grains that poikolitically enclose quartz and feldspar near their margins. Grains have long dimensions that vary within each specimen from 30 to a maximum of 500–2000 microns. There is no

Table 1. Comparison of composition of andesite from Mount Hood determined in the XRF laboratory, Department of Chemistry, Arizona State University with composition of same material determined at Technical Service Laboratories.

	ASU	TSL	% difference relative to ASU value
SiO_2	60.56	58.99	2.6
Al_2O_3	18.09	17.89	1.1
Fe_2O_3	6.42	7.00	9.0
CaO	6.15	6.53	6.2
MgO	2.88	2.83	1.7
Na_2O	4.32	4.54	5.1
K_2O	1.09	0.91	16.5
TiO_2	0.94	1.00	6.4
MnO	0.12	0.10	16.7
P_2O_5	0.22	0.21	4.5

Table 2. Mineral assemblage and mineral composition data for graphitic sulfide-rich schists*

Major Minerals	Chlorite Zone		Biotite Zone		Garnet Zone		Staurolite + Andalusite Zone				
	272B	1111A	274A	274B	196A	1122G	240A	919G	1005A	1007B	1011A
quartz	x	x	x	x	x	x	x	x	x	x	x
pyrite	x	o	x	o	x	x	x	o	x	x	x
pyrrhotite†	0.898	0.895	0.892	0.906	x	0.916	0.899	0.916	0.900	0.896	0.902
biotite§	o	o	0.055	0.119	0.056	0.047	0.047	0.378	0.042	0.046	0.035
dolomite§	0.100	0.158	0.064	o	o	o	o	o	o	o	o
plagioclase††	0.01	0.01	0.37	0.32	0.40	0.47	0.51	0.42	0.57	0.55	0.75
K-feldspar§§	o	o	o	o	o	0.95	0.95	o	o	0.95	o
muscovite§§	0.95	0.95	o	0.97	0.98	o	o	0.85	0.96	o	o
Accessory Minerals											
chlorite§	o	o	0.063	o	o	o	o	o	o	o	o
prehnite	o	o	o	o	o	x	x	o	x	x	x
rutile	x	x	x	x	o	x	o	x	x	x	x
sphene	o	o	o	o	x	x	x	o	o	x	x
chalcopyrite	x	x	x	x	x	x	x	x	x	x	x
graphite**	x	x	x	x	x	x	x	x	x	x	x
calcite§	o	0.24	o	o	o	o	o	o	o	o	o
siderite#	o	o	Fe0.88 Mn0.02 Ca0.10	Fe0.91 Mn0.04 Ca0.05	o	o	o	o	o	o	o

Major Minerals	Sillimanite Zone							
	711B	965A	967A	970A	1103-1	1106-1	1107-1	1107-2
quartz	x	x	x	x	x	x	x	x
pyrite	o	o	x	o	x	o	o	o
pyrrhotite †	0.940	0.892	0.909	0.920	0.894	0.918	0.912	0.918
biotite§	0.311	0.074	0.018	0.467	0.048	0.157	0.181	0.148
dolomite§	o	o	o	o	o	o	o	0
plagioclase††	0.72	0.88	0.93	0.92	0.85	0.41	0.44	0.89
K-feldspar§§	0.96	x	o	0.93	0.93	0.94	o	o
muscovite§§	0.98	o	o	o	o	0.97	0.95	o
Accessory Minerals								
chlorite§	o	o	o	o	o	o	o	o
prehnite	x	o	o	o	o	o	o	o
rutile	x	x	x	o	o	x	x	x
sphene	x	o	o	x	x	o	x	x
chalcopyrite	x	x	x	x	x	x	x	x
graphite**	x	x	x	x	x	x	x	x
calcite§	o	o	o	o	o	o	o	o
siderite#	o	o	o	o	o	o	o	o

** x=present; o=absent; ** graphite or graphitic material; † z, Fe_zS; †† X_{an}; § Fe/(Fe+Mg); §§ K/(K+Na); # Molar proportions of Fe, Mn, and Ca components.*

systematic change in grain size with increasing metamorphic grade. In some samples large pyrrhotite grains tend to be aligned in discontinuous layers with the distance between layers 2–5 mm. Pyrrhotite ranges in composition from $Fe_{0.89}S$ to $Fe_{0.94}S$. Although sulfides were analyzed for Fe and S only, the sum Fe + S suggests that elements other than Fe and S, if present, occur in concentrations less than 1 weight percent. Comparison of the measured composition of pyrrhotite coexisting with pyrite (Table 2) with the data of Toulmin and Barton (1964) indicates that pyrrhotite compositions have changed following metamorphism as is commonly observed elsewhere (*e.g.*, Guidotti, 1970a). Some pyrrhotite in most specimens is slightly altered to marcasite along fractures (*cf.* Ramdohr, 1969, Fig. 415). The alteration is attributed to surficial weathering and affects less than 3% of pyrrhotite in all samples except 240A.

Table 3. Modal percent pyrite, pyrrhotite, and biotite in graphitic sulfide-rich schists

Specimen Number	Percent Pyrite	Percent Pyrrhotite	Percent Biotite
272B	1.7	6.0	0
1111A	0	2.7	0
274A	1.0	10.4	nd*
274B	0	2.3	nd*
196A	14.5	tr	nd*
1122G	10.7	3.8	25.7
240A	0.6	4.8	23.8
919G	0	3.1	nd*
1005A	8.9	3.3	nd*
1007B	8.6	4.4	20.6
1011A	8.1	7.0	25.5
711B	0	5.5	24.9
965A	0	2.4	nd*
967A	0.3	11.1	25.6
970A	0	4.6	34.8
1103-1	0.2	10.9	14.7
1106-1	0	5.9	5.0
1107-1	0	6.5	nd*
1107-2	0	4.3	nd*

* *not determined*

Although both monoclinic and hexagonal pyrrhotite are reported from the study area (Williamson and Meyer, 1969), no systematic attempt to characterize pyrrhotite in this manner was made. Petrographic examination of selected polished samples coated with a fine-grained magnetite precipitate (Scott, 1974) indicated that all or almost all pyrrhotite is hexagonal.

Ten samples contain pyrite which occurs as subhedral or euhedral grains that frequently contain strings of inclusions that are oriented parallel to foliation. Euhedral grains form squares or rectangles in thin section with dimensions that vary in each specimen from 30–3000 microns. The grain size of pyrite does not systematically change as a function of metamorphic grade. Some but not all pyrite occurs as inclusions within pyrrhotite. No rims of pyrite around grains of pyrrhotite, such as those described by Guidotti (1970a), were observed in rocks of this study. Several analyses of pyrite indicate that it is stoichiometric FeS_2 with less than one weight percent elements other than Fe and S. Approximately 5% of the pyrite in two sections (196A and 1007B) is partially altered to limonite (*cf.* Ramdohr, 1969, Fig. 480).

Pyrite, pyrrhotite, and the silicate and carbonate minerals are intimately integrown in all samples of graphitic sulfide-rich schist. No textural features were observed in thin section that would suggest disequilibrium either between pyrite and pyrrhotite or between sulfides and silicates.

All samples contain chalcopyrite which occurs as anhedral equant grains 10–30 microns in diameter and in close association with pyrrhotite.

Graphitic material

All specimens contain graphitic material. In the chlorite, biotite, garnet, and staurolite + andalusite zones it occurs as minute (< 5 microns) grains of unknown crystalline character along grain boundaries between silicates and sulfides. The graphitic matter is distributed evenly throughout most samples, but in a few specimens it is concentrated in 5–10 micron layers that are separated by approximately 50 microns. In the sillimanite zone, rocks contain well-crystallized grains of graphite which have long dimensions of approximately 50 microns.

Sheet silicates

All rocks in the biotite zone and at higher grades contain biotite. In specimens from the biotite, garnet, and staurolite + andalusite zones, biotite is evenly distributed throughout specimens but occurs in two sizes. Most biotite is subhedral with a long dimension near 70 microns. Near sulfide grains, however, biotite grains are much larger, typically 200 microns long. In samples from the sillimanite zone, however, biotite is of roughly uniform size everywhere in thin section with a long dimension of 300–1000 microns. Representative chemical analyses of biotite are given in Table 4. All analyses in Table 4 represent averages of 2–6 individual determinations from a thin section of one sample. Analyzed biotites are distinctive in their wide range in composition: Fe/(Fe+Mg) ranges from 0.02–0.47.

Muscovite occurs in all samples from the chlorite zone and in seven samples collected from the other zones at higher grades. In rocks in the chlorite, biotite, garnet, and staurolite + andalusite zones muscovite is evenly distributed as subhedral grains 100 microns long. No large muscovite grains were observed near sulfide grains. In sillimanite zone samples the long dimension of muscovite is much larger, 500 microns. Representative muscovite compositions are listed in Table 4.

One sample (274A) contains chlorite whose composition is listed in Table 4. Chlorite forms subhedral grains, 200 × 70 microns in size, and is always associated with large biotite crystals near grains of sulfide.

Six samples contain traces of prehnite that occurs

Table 4. Compositions of selected sheet silicates from graphitic sulfide-rich schists

	Biotites								Muscovites			
	274A	196A	1122G	1007B	711B	967A	1103-1	1107-1	272B	274B	1005A	1107-1
TiO_2*	0.51	0.52	0.39	1.04	1.87	1.19	1.23	1.79	0.42	0.34	1.69	1.70
MnO	0.13	0.26	0.12	0.75	0.62	0.20	0.51	0.53	0.03	0.04	0.03	0.01
FeO	2.39	2.39	1.96	1.91	11.71	0.80	1.98	7.01	2.25	1.33	0.79	0.59
Na_2O	0.12	0.05	0.03	0.04	0.04	0.08	0.10	0.15	0.36	0.22	0.30	0.39
MgO	22.81	22.56	22.46	22.15	14.50	23.53	21.97	17.72	1.26	3.65	1.87	1.48
Al_2O_3	18.12	18.27	18.83	19.13	18.75	18.24	18.49	19.71	33.60	26.71	33.06	34.05
SiO_2	42.65	41.45	42.11	41.17	38.96	41.78	41.89	39.76	49.05	52.13	47.42	46.28
K_2O	9.57	9.87	9.54	9.76	9.84	9.98	9.88	9.79	9.23	10.22	10.57	10.82
CaO	0.00	0.00	0.00	0.00	0.00	0.00	0.00	0.01	0.00	0.00	0.00	0.00
Sum	96.28	95.36	95.41	95.95	96.30	95.80	96.05	96.47	96.17	94.78	95.71	95.33
K**	0.836	0.874	0.840	0.859	0.906	0.874	0.869	0.878	0.769	0.867	0.892	0.918
Na	0.015	0.006	0.004	0.004	0.004	0.009	0.012	0.019	0.045	0.027	0.038	0.050
Fe	0.136	0.138	0.112	0.110	0.706	0.045	0.113	0.411	0.122	0.073	0.044	0.031
Mg	2.331	2.337	2.309	2.280	1.562	2.412	2.257	1.860	0.122	0.361	0.185	0.147
Mn	0.006	0.014	0.006	0.043	0.036	0.010	0.028	0.030	0.001	0.000	0.002	0.000
Ti	0.026	0.026	0.020	0.053	0.100	0.059	0.062	0.093	0.020	0.016	0.084	0.084
Al	0.386	0.377	0.434	0.399	0.412	0.351	0.388	0.432	1.796	1.563	1.714	1.750
Al	1.077	1.119	1.096	1.157	1.184	1.127	1.113	1.202	0.793	0.532	0.864	0.920
Si	2.923	2.881	2.904	2.843	2.816	2.873	2.887	2.798	3.207	3.468	3.136	3.080

	Chlorite		Prehnites		
	274A		1122G	1005A	1007B
TiO_2*	0.00	TiO_2*	0.07	0.49	0.15
MnO	0.19	MnO	0.07	0.31	0.45
FeO	3.65	FeO	0.28	0.64	0.32
Na_2O	0.01	Na_2O	0.00	0.03	0.02
MgO	30.33	MgO	0.22	0.32	1.54
Al_2O_3	23.08	Al_2O_3	24.60	23.89	24.13
SiO_2	30.35	SiO_2	43.72	43.24	43.68
K_2O	0.07	K_2O	0.02	0.04	0.03
CaO	0.00	CaO	26.90	25.94	25.03
Sum	87.68	Sum	95.85	94.89	95.40
$Fe^{\#}$	0.283	Ca**	1.974	1.928	1.842
Mg	4.219	Mg	0.021	0.034	0.157
Mn	0.013	Fe	0.015	0.037	0.018
Ti	0.000	Mn	0.002	0.018	0.025
Al	2.537	Ti	0.001	0.026	0.007
Si	2.831	Al	1.986	1.954	1.953
		Si	2.996	3.000	3.001

** oxide weight percents; ** cations/11 anhydrous oxygen atoms; # cations/14 anhydrous oxygen atoms.*

as fan-like aggregates. Representative chemical analyses of prehnite are given in Table 4. The origin of the prehnite is uncertain. It only occurs in rocks metamorphosed to garnet zone conditions or to higher grades. Its peculiar crystal habit, however, suggests that it may be a retrograde product.

Feldspars and quartz

All specimens contain plagioclase feldspar. In rocks from the chlorite, biotite, garnet, and staurolite + andalusite zones plagioclase occurs as anhedral, equant grains 10–30 microns in diameter. In sillimanite zone rocks plagioclase is larger, 50–70 microns in diameter. All plagioclase in chlorite zone samples is almost pure albite (Table 2). Plagioclase becomes increasingly calcic in composition with increasing metamorphic grade; some specimens collected in the sillimanite zone contain anorthite (An_{90-95}).

Seven samples contain microcline and they all were collected in the garnet zone or at higher metamorphic grades. In samples from the garnet and

staurolite + andalusite zones microcline occurs in ovoid spots 500–1000 microns in diameter. Some spots are single feldspar crystals while some are aggregates of 5–10 feldspar grains. The ovoid spots include other minerals, usually some combination of large biotite grains, quartz, pyrrhotite, and pyrite. In samples collected in the sillimanite zone, microcline is comparable in size and shape with plagioclase feldspar (equant and 50–70 microns in diameter). Analyzed microclines are K–Na compounds but with a very restricted composition, X_{or} = 0.93–0.96 (Table 2).

Quartz occurs in all samples. In specimens from the chlorite, biotite, garnet, and staurolite + andalusite zones it is observed in two size ranges. Most quartz is anhedral, equant, and 10–30 microns in diameter. Some larger quartz grains (100–300 microns in diameter) are closely associated with pyrite and pyrrhotite. Sillimanite zone samples contain quartz of more uniform size, 50–100 microns in diameter.

Carbonates

Both samples collected in the chlorite zone and one in the biotite zone contain ferroan dolomite. Dolomite is evenly distributed through the rock as grains 30–50 microns in diameter. Compositionally the dolomite is close to a $Ca(Fe,Mg)(CO_3)_2$ solid solution with measured Fe/(Fe+Mg) = 0.06–0.16 (Table 2). One sample (1111A) contains calcite grains 20–30 microns in diameter.

Both specimens collected in the biotite zone contain siderite which occurs in aggregates of equant 50–70 micron diameter grains which partially rim some pyrrhotite grains and which are intergrown with large biotite and chlorite crystals. The siderite occurs in small amounts (<1 modal percent). It appears to replace pyrrhotite and may be a retrograde product. Siderite is a $(Fe,Ca,Mn)CO_3$ solid solution with composition listed in Table 2.

Ti-rich minerals

All samples contain rutile and/or sphene. Rocks in the chlorite and biotite zone only contain rutile which occurs as anhedral, poikolitic grains 10–30 microns in diameter. Rutile retains the same crystal size and shape in garnet and staurolite + andalusite zone samples. In the sillimanite zone specimens rutile forms subhedral grains with long dimensions of approximately 100 microns. Sphene occurs in some samples collected in the garnet, staurolite + andalusite, and sillimanite zones as subhedral grains 40–60 microns in their long dimensions. The composition of rutile and sphene was not determined.

Mineral assemblages; changes in mineralogy with metamorphic grade

Mineral assemblages observed in the graphitic sulfide-rich schists in each of the metamorphic zones are summarized below. Accessory minerals are in parentheses.

Chlorite Zone: muscovite + ferroan dolomite + quartz + albite + pyrrhotite ± pyrite (+ rutile + chalcopyrite + graphitic material).

Biotite Zone: biotite + quartz + andesine + pyrrhotite ± pyrite ± muscovite ± ferroan dolomite (+ rutile + chalcopyrite + graphitic material + siderite ± chlorite).

Garnet Zone: biotite + quartz + andesine + pyrrhotite + pyrite ± muscovite ± microcline (+ sphene + chalcopyrite + graphitic material ± rutile ± prehnite).

Staurolite + Andalusite Zone: biotite + quartz + andesine/bytownite + pyrrhotite ± pyrite ± muscovite ± microcline (+ chalcopyrite + graphitic material ± rutile ± sphene ± prehnite).

Sillimanite Zone: biotite + quartz + andesine/anorthite + pyrrhotite ± pyrite ± muscovite ± microcline (+ chalcopyrite + graphite ± rutile ± sphene ± prehnite).

The principal changes in mineralogy of the graphitic sulfide-rich schists occur over the transition from chlorite to garnet zone conditions. In this interval the metamorphic rocks develop biotite, microcline, and sphene while ferroan dolomite is eliminated. At garnet zone conditions and at higher grades the schists contain a very simple mineralogy (ignoring accessory phases) that does not systematically change as a function of grade: plagioclase + biotite + quartz + pyrrhotite ± pyrite ± muscovite ± microcline. The compositions of some minerals change with metamorphic conditions. Plagioclase systematically becomes more calcic with increasing grade of metamorphism. Although magnesian biotites are found in some rocks at all grades, biotite with Fe/(Fe+Mg) > 0.2 is found only in rocks from the staurolite + andalusite and sillimanite zones. Proportions of some minerals change as a function of metamorphic grade. The most significant of these changes is the ratio of pyrite to pyrrhotite; the ratio is very low (0.00–0.02) in all samples collected in the sillimanite zone compared to the ratio in one or more samples collected at lower grades.

Whole-rock chemistry

Chemical analyses of the 19 graphitic sulfide-rich schists are listed in Table 5. During analysis of the

whole-rock samples, iron is oxidized to Fe_2O_3; consequently total iron is reported as Fe_2O_3.

Much iron in the rock samples, however, is bound in sulfide rather than in oxide compounds. Representation of total iron in Table 5 as Fe_2O_3 artificially adds oxygen to the analysis that actually is not contained in the rock (the same would occur if total iron were represented as FeO). Consequently, for many rocks in Table 5, the sum of metal oxide, sulfur, and carbon weight percents is greater than 100%. Sums greater than 100% are an artifact of representing total iron as an iron oxide rather than as a combination of iron oxide and iron sulfide. It would have been most accurate to represent total iron in Table 5 as an appropriate combination of Fe_2O_3, FeO, FeS, and FeS_2. This was not possible both because the rock samples were not analyzed for oxygen and because whole-rock ferric–ferrous ratios were not determined. Fortunately, the arguments that follow require only a knowledge of total whole-rock iron and sulfur contents and not of how the iron is distributed between various sulfide and oxide compounds.

Analysts at Technical Service Laboratories obtained poor yields during loss on ignition for samples that contain appreciable carbonate (A. Debnam, personal communication, 1980). Consequently the sums for samples 272B, 274A, and 1111A are slightly low (97–98%). Analysis of the metallic element constituents by inductively coupled argon plasma methods, however, is not dependent on a determination of LOI. The measured concentrations of metals in samples 272B, 274A, and 1111A, therefore should be reliable.

Values for sulfur in Table 5 represent an unweighted average of two duplicate analyses by C. F. Lewis at Arizona State University and one analysis by A. Debnam at Technical Service Laboratories. The individual measurements deviated from the average usually by no more than ±0.5 weight percent. Sulfur analyses for four samples in Table 5 are unlikely to be reliable. Samples 196A, 1007B, and 1107-2 contain some sulfide grains partially converted to limonite during surficial weathering. Consequently their given sulfur contents are likely to be too low relative to the unaltered metamorphic rock. Sample 240A contains an appreciable number of pyrrhotite grains partially converted to marcasite during surficial weathering. Consequently its stated sulfur content is likely to be too high relative to the unaltered metamorphic rock.

Student's t test (Leabo, 1972) was used in conjunction with the data in Table 5 to evaluate whether the schists underwent any statistically significant changes in their content of major metal oxides (SiO_2, Al_2O_3, Fe_2O_3, MgO, CaO, Na_2O, K_2O, TiO_2) as a function of metamorphic grade. Differences were taken as significant if they occurred at a >95% confidence level. With the exception of Na_2O, average major metal oxide contents of rocks (on a volatile-free basis) within a particular metamorphic zone are not significantly different from average metal oxide contents in each of the other four zones. The difference in average Na_2O content between chlorite and sillimanite zone rocks is significant at a >99.9% confidence level. Ferry (1980c) noticed a similar, statistically significant, decrease in the sodium content of metamorphosed carbonate rocks with increasing metamorphic grade in the study area of Figure 1. The sample base in Table 5 may be too small, however, to confidently conclude that the schists lost sodium during the metamorphic event. It is safe to say that, within the context of the sample population, the rocks collected for this study are at least broadly isochemical with respect to major non-volatile elements except possibly sodium.

Attainment of equilibrium

It will be assumed in later sections that chemical equilibrium was attained among major minerals in the graphitic sulfide-rich schists during the peak of metamorphism. A variety of observations are consistent with that assumption. Silicate and carbonate mineral grains appear fresh in thin section. Some sulfide grains are altered but alteration products are usually minute in volume compared to the volume of fresh-looking sulfide. Mineral grains have sharp, smooth boundaries. With the exception of pyrite inclusions in pyrrhotite, there is no textural evidence for reaction relationships between minerals in the samples. Individual mineral grains are homogeneous in composition, and there is little or no variation in mineral composition from one portion of a thin section to another.

If an equilibrium relationship can be written among chemical potentials of components in Fe–Mg silicates, sulfides, and other coexisting phases, then compositions of Fe–Mg silicates and sulfides can be represented on a diagram such as Figure 2 (Popp *et al.*, 1977). Minerals, whose compositions are portrayed in Figure 2, are part of the assemblage biotite + microcline + pyrrhotite ± pyrite. The requisite equilibrium relationship is:

$$\mu_{KFe_3AlSi_3O_{10}(OH)_2,\text{biotite}} + 3\mu_{H_2S,\text{fluid}} = \mu_{KAlSi_3O_8,\text{K-feldspar}} + 3\mu_{FeS,\text{pyrrhotite}} + 4\mu_{H_2O,\text{fluid}} \quad (1A)$$

Table 5. Whole-rock chemical data for graphitic sulfide-rich schists

	Chlorite Zone		Biotite Zone		Garnet Zone		Staurolite + Andalusite Zone				
	272B	1111A	274A	274B	196A	1122G	240A	919G	1005A	1007B	1011A
SiO_2*	58.57	67.02	54.61	77.20	55.40	53.23	55.28	55.89	60.37	55.73	57.30
Al_2O_3	14.40	9.43	13.24	9.64	13.22	13.09	16.24	18.66	12.11	13.31	10.23
Fe_2O_3**	9.25	4.50	13.12	4.64	11.35	13.22	5.19	8.89	12.13	12.32	14.98
CaO	2.54	4.81	2.61	0.70	2.43	3.73	4.09	2.70	1.62	3.50	3.50
MgO	3.06	2.66	3.46	2.98	3.54	4.23	5.51	3.84	2.53	3.25	3.58
Na_2O	1.81	2.07	0.73	0.20	1.06	1.52	1.92	2.17	0.45	1.13	0.67
K_2O	3.19	1.71	3.57	2.10	3.30	2.45	4.12	3.52	2.95	3.49	1.51
TiO_2	0.72	0.61	0.73	0.54	0.78	0.83	0.82	0.95	0.69	0.80	0.58
MnO	0.07	0.07	0.08	0.03	0.05	0.06	0.17	0.10	0.08	0.11	0.12
P_2O_5	0.10	0.06	0.08	0.07	0.05	0.09	0.07	0.07	0.07	0.07	0.06
LOI†	3.66	4.60	4.96	1.98	8.50	7.57	5.24	1.72	7.13	5.66	7.43
Sum	97.37	97.53	97.19	100.08	99.68	100.02	98.65	98.51	100.13	99.37	99.96
S	3.51	1.30	5.40	1.46	8.12§	9.92	2.95§	1.57	7.72	5.80§	9.26
C	1.54	2.31	1.91	0.12	1.46	0.75	2.35	0.03	1.68	0.90	2.04

	Sillimanite Zone							
	711B	965A	967A	970A	1103-1	1106-1	1107-1	1107-2
SiO_2*	55.41	76.61	58.61	52.94	59.07	53.85	60.30	53.90
Al_2O_3	17.68	9.68	12.96	19.33	12.56	20.98	16.65	18.26
Fe_2O_3**	10.56	4.25	11.59	10.80	12.25	8.99	9.70	8.75
CaO	6.06	3.86	4.10	8.28	4.70	1.85	1.56	5.86
MgO	3.43	2.13	6.13	3.41	3.78	1.78	2.58	6.15
Na_2O	0.79	0.22	0.14	0.24	0.40	1.28	0.91	0.42
K_2O	3.48	0.85	2.50	2.59	2.01	6.29	4.47	3.33
TiO_2	0.88	0.86	0.72	1.00	0.68	1.07	0.99	0.96
MnO	0.14	0.08	0.11	0.16	0.12	0.04	0.08	0.17
P_2O_5	0.10	0.07	0.11	0.12	0.08	0.10	0.08	0.15
LOI†	1.72	1.17	2.62	1.33	4.47	3.06	2.77	2.07
Sum	100.25	99.78	99.59	100.20	100.12	99.29	100.09	100.02
S	3.26	nd§§	4.96	2.48	5.92	2.93	3.87	2.43§
C	0.33	nd§§	0.54	0.58	1.60	0.43	0.47	0.54

** weight percent; ** all Fe as Fe_2O_3; † loss on ignition; § contains weathered sulfide; §§ not determined.*

Data for samples from the garnet, staurolite + andalusite, and sillimanite zones are all plotted. There is a systematic relation between the composition of biotite and the identity of iron sulfides in the rocks. All rocks with pyrite + pyrrhotite + microcline contain biotite with measured Fe/(Fe+Mg) = 0.046–0.048. All rocks with pyrrhotite + microcline but without pyrite contain more iron-rich biotite with measured Fe/(Fe+Mg) = 0.16–0.47. The regular relationship between biotite and sulfide compositions, illustrated in Figure 2, is a strong argument for attainment of chemical equilibrium among sulfides and silicates during metamorphism. The limited crossing of two tie lines in Figure 2 is probably caused by adjustment of pyrrhotite compositions to post-metamorphic conditions.

A number of features that are evidence for a departure from chemical equilibrium should be mentioned. As noted above, pyrrhotite grains do not have the compositions they did during the metamorphic event. Pyrrhotite rarely, if ever, retains peak metamorphic compositions. Sulfides in almost all samples show signs of surficial weathering. Secondary marcasite, however, constitutes <3% of the sulfides in all samples but 240A; secondary limonite occurs in volumes <1% of sulfide volumes in all samples but 196A, 1007B, and 1107-2. The textures of siderite and prehnite suggest that they may have grown after the peak of metamorphism. The evidence for disequilibrium is not taken as a serious objection to the assumption of chemical equilibrium among major minerals in the graphitic sulfide-rich schists. Marca-

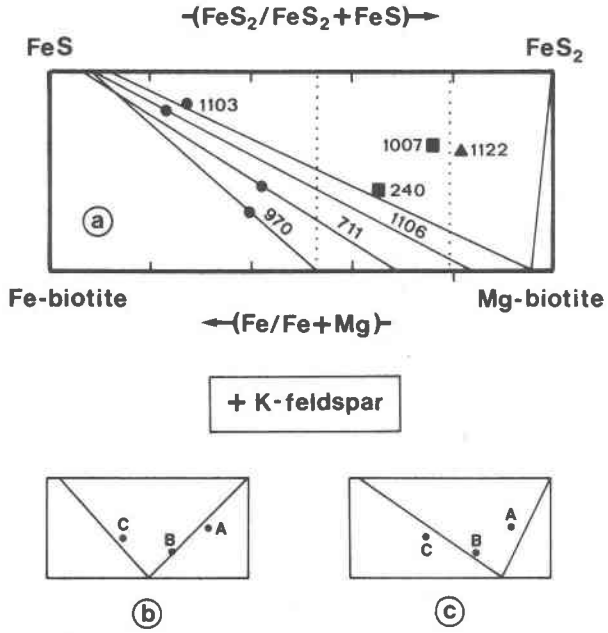

Fig. 2. Chemographic relations among coexisting biotite and iron sulfides in samples of graphitic sulfide-rich schist that contain K-feldspar. a. Solid lines are tie lines for specimens collected in the study area (sample numbers refer to Fig. 1). Filled symbols represent the bulk composition of the samples determined from modes and mineral composition data. Circles: sillimanite zone rocks; squares: staurolite + andalusite zone rocks; triangles: garnet zone rocks. Vertical dotted lines separate samples from different metamorphic zones. Samples 240A, 1007B, 1103-1, and 1122G define the same pyrite-pyrrhotite-biotite triangle within error of measurement. b. and c. Hypothetical change in the position of the pyrite–pyrrhotite–biotite triangle with increasing grade of metamorphism if the pyrite–pyrrhotite transition were to involve sulfide–silicate reactions.

site, limonite, siderite, and prehnite occur in very small amounts (<1%). Furthermore, there is abundant evidence for attainment of equilibrium among minerals in metacarbonate rocks interbedded with the graphitic sulfide-rich schists in the area of Figure 1 (Ferry, 1976a, 1979). It seems reasonable, therefore, to assume that chemical equilibrium was closely attained in the graphitic sulfide-rich schists as well.

Fluid compositions

The composition of a C–O–H–S fluid in equilibrium with the assemblage biotite + graphite + K-feldspar + pyrite + pyrrhotite was calculated for four specimens (Table 6). Calculations are based on procedures developed by Eugster and Skippen (1967) and Skippen (1971) for C–O–H fluids. Conditions of $P_{fluid} = P_{total} = 3500$ bars and ideal mixing of components in the fluid were assumed. Sources of fugacity coefficients are those listed in Ferry (1976b). Thermodynamic data for H_2O, CO_2, CO, H_2S, and CH_4 were taken from the compilation of Stull and Prophet (1971). The temperature of equilibrium was estimated using biotite–garnet geothermometry in nearby pelitic schists (Ferry, 1980b). Sulfur fugacity data were taken from Toulmin and Barton (1964) at the estimated temperature of equilibrium and corrected for a pressure of 3500 bars. The final constraint needed to calculate fluid composition is the relation between f_{H_2O} and f_{H_2S} prescribed by equilibrium 1A. Following the analysis of Ferry (1976b), a numerical expression for the equilibrium represented by equation 1A may be derived:

Table 6. Calculated composition of C–O–H–S fluids in equilibrium with graphitic sulfide-rich schists during metamorphism

Specimen Number	T(°C)	$-\ln f_{S_2}$	$-\ln f_{O_2}$	X_{H_2O}	X_{CO_2}	X_{CH_4}	X_{H_2S}	X_{H_2}
1122G	450°	12.723	63.482	0.242	0.000	0.738	0.015	0.005
1007B	475°	11.050	61.745	0.442	0.001	0.520	0.033	0.004
240A	480°	10.727	60.842	0.507	0.001	0.450	0.037	0.004
1103-1	540°	7.206	50.906	0.709	0.229	0.011	0.050	0.001

$$28{,}563 - 69.850T(°K) - 0.233P(\text{bars}) + RT\ln K_s + 4RT\ln f_{H_2O} - 3RT\ln f_{H_2S} = 0, \quad (1B)$$

where

$$K_s = (a_{FeS,po})^3(a_{or,kf})/(a_{ann,bio}).$$

The first two terms in (1B) were derived from the experimental data of Tso *et al.* (1979) using procedures outlined by Ferry (1976b). The third term was derived from data in Robie *et al.* (1967). Activities were either estimated from mineral composition data (Table 2) and simple activity–composition models (biotite, Ferry, 1976b), or for sulfides, taken from data in Toulmin and Barton (1964) corrected for a pressure of 3500 bars.

The principal species that compose the fluids in equilibrium with the graphitic sulfide-rich schists are CH_4, H_2O, and CO_2. Graphitic sulfide-rich schists in the garnet and in the staurolite + andalusite zones were in equilibrium with nearly binary CH_4–H_2O mixtures. The ratio H_2O/CH_4 appears to have increased with increasing grade (temperature). Fluids in the sillimanite zone appear to be close to binary CO_2–H_2O mixtures with very little CH_4.

Pyrite–pyrrhotite relations

Iron sulfides in sediments and sedimentary rocks

Some ensuing arguments regarding the behavior of iron sulfides during metamorphism are based on ob-

served occurrences of iron sulfides in sediments and sedimentary rocks. It is useful, therefore, to briefly review the origin of iron sulfides in sediments and their occurrence in sedimentary rocks. The protoliths of the graphitic sulfide-rich schists were almost certainly black shales which, in turn, represent lithified anoxic muds. The formation of iron sulfide in marine anoxic muds has been thoroughly studied (Kaplan *et al.,* 1963; Berner, 1964; Berner, 1970; Sweeney and Kaplan, 1973; Goldhaber *et al.,* 1977; Berner *et al.,* 1979). Iron and sulfur first combine during diagenesis in anoxic muds to form various amorphous and metastable iron monosulfides (*e.g.,* mackinawite and greigite). The iron monosulfides react with sulfide, produced by the reduction of seawater sulfate, to form pyrite. Reduction of sulfate to sulfide is usually accomplished by anaerobic bacteria but apparently may also occur abiotically (Sweeney and Kaplan, 1973). The conversion of iron monosulfides is usually 95–100% complete at depths greater than one meter below the sediment–seawater interface (Berner, 1964; Goldhaber *et al.,* 1977). The complete conversion of iron monosulfide to pyrite, observed in modern anoxic muds, must also have occurred at least as far back as the beginning of the Paleozoic Era. Standard texts on sedimentary rocks (*e.g.,* Milner, 1962; Greensmith *et al.,* 1971) as well as comprehensive reviews in journals (*e.g.,* Love and Amstutz, 1966; Vallentyne, 1963) are testimony to the abundance of pyrite in Phanerozoic marine sedimentary rocks. In contrast, detailed studies of pyritic black shales usually report the complete absence of pyrrhotite (*e.g.,* Bates and Strahl, 1957; Elverhøi, 1977). Reviews of the occurrence of pyrrhotite in sedimentary rocks (Rosenthal, 1956; Kaplan *et al.,* 1963) conclude that, while pyrrhotite is observed in marine sedimentary rocks, it is very rare. Examination of the actual published descriptions reveal that pyrrhotite is found in sedimentary rocks in two kinds of occurrences. One is pyrrhotite in black shales and marine limestones where pyrite occurs in far greater abundance (Oftedahl, 1955; Rubey, 1930). The second is pyrrhotite as inclusions within calcite crystals that cover quartz-lined geodes in marine limestones (Smyth, 1911; Erd *et al.,* 1957). From studies of anoxic muds and black marine shales in the literature, I conclude that all or almost all iron sulifde in marine black shales is pyrite. This conclusion is supported by studies of low-grade metamorphic rocks. Carpenter (1974) observed that black phyllites, studied from a chlorite zone, contained pyrite only. Although French (1968) investigated a different rock type, he similarly observed only pyrite in low-grade metamorphosed iron-formation.

The graphitic sulfide-rich schists in the study area contain graptolites (Osberg, 1968), and are probably metamorphic equivalents of pyritic marine black shales. Because there is no evidence that pyrrhotite exists in more than trace quantities in marine black shales, I will assume that *all* iron sulfide originally in the rocks was in the form of pyrite. The studies of sediments and sedimentary rocks, cited above, are evidence that pyrrhotite observed in rocks from the chlorite zone of Figure 1 and at higher grades is formed by metamorphic mineral reactions.

A final noteworthy characteristic of pyritic marine black shales is that all or almost all iron in the rock is combined with sulfur as pyrite. Conant and Swanson (1961) report the chemical analysis of a sample of the Chattanooga shale, a marine black shale containing 10–15 modal percent pyrite and only traces of other sulfides (*e.g.,* chalcopyrite and sphalerite). If it is assumed (as seems appropriate) that all sulfur in the rock is in the form of pyrite, then the chemical analysis requires that 90% of the rock's iron is bonded to sulfur as pyrite. If the stated values for iron and sulfur in the analysis are in error by ±5% relative, then 81–99% of the rock's iron resides in pyrite. Pettijohn (1973) reports the chemical composition of six black shales, four of which are sulfur-rich (>1 wt.% S). One sample is a Devonian black shale from Georgia. Even allowing a ±5% relative error for stated values of sulfur and iron in the analysis, 100% of the iron in the shale must be combined with sulfur as pyrite. Allowing ±5% relative error for stated values of sulfur and iron, the mole percent iron that resides in pyrite in the other three samples is: 84–87% (Devonian black shale from Ohio); 90–92% (Precambrian graphitic slate from Michigan); and 100% (Posidienschiefer, Germany). One sample of graphitic sulfide-rich schist from the present study area (196A) contains only traces of sulfide other than pyrite. From the chemical analysis of sample 196A (Table 5), allowing ±5% relative error for stated iron and sulfur values, 81–98% of the rock's iron apparently resides in pyrite. The percentage derived from chemical analysis of sample 196A is probably too low because, as discussed above, the stated sulfur content for the sample is likely too low. A more accurate estimate of the amount of iron combined with sulfur in the rock can be derived from modal and mineral composition data. Sample 196A contains 14.5 modal percent pyrite and 35.7 modal percent muscovite + biotite (it is difficult to distinguish fine-grained mag-

nesian biotite from muscovite during modal analysis). If all mica is biotite, then using the chemical analysis of biotite in Table 4, a maximum of 0.33 moles iron/1000 cm^3 rock resides in mica. The rock contains no other Fe–Mg silicates. Pyrite contains 6.06 moles iron/1000 cm^3 rock. More than 95% iron in sample 196A therefore resides in pyrite. Based on chemical analyses of pyritic black shales and on the analysis of sample 196A, I will assume that all iron in the unmetamorphosed equivalents of the graphitic sulfide-rich schists was bonded to sulfur as pyrite.

Pyrite–pyrrhotite isograds

Carpenter (1974) reported a pyrite–pyrrhotite isograd which almost exactly coincided with a biotite isograd mapped in pelitic schists. At grades lower than the pyrite–pyrrhotite isograd, rocks contain pyrite and lack pyrrhotite. At grades higher than the isograd the rocks contain pyrrhotite without pyrite.

Data in Tables 2 and 3 demonstrate that a pyrite–pyrrhotite isograd cannot be mapped in the study area. All rocks, including those in the chlorite zone contain substantial amounts of pyrrhotite. Some rocks in all zones contain pyrite. Guidotti (1970a) similarily observed that pyrite + pyrrhotite are widely distributed in schists collected from different metamorphic grades.

The pyrite–pyrrhotite transition

In order to determine whether there exists a reaction relationship between pyrite and pyrrhotite in the graphitic sulfide-rich schists, the molar ratios of pyrite/(pyrite + pyrrhotite) were calculated from modal data (Table 3) and plotted as crosses (Fig. 3) as a function of metamorphic grade. There is, of course, a wide variation in pyrite/(pyrite + pyrrhotite), but the ratio does appear to be lower, on the average, for samples collected in the sillimanite zone than for samples collected in the other zones. The data in Figure 3 for the graphitic sulfide-rich schists are, in part, unrevealing because so few samples constitute the data base. The relationship between pyrite and pyrrhotite during progressive metamorphism of pelitic rocks can be more readily seen by examination of data for 59 normal schists collected in the study area as well as the 19 graphitic sulfide-rich schists (small dots, Fig. 3). As with data for the graphitic sulfide-rich rocks, there is a wide variation in molar pyrite/(pyrite + pyrrhotite) in each zone (as expressed by the large standard deviations in Fig. 3). The *average* pyrite/(pyrite + pyrrhotite), for each zone, however, continuously decreases with increasing metamorphic grade from chlorite zone to sillimanite zone conditions. Some differences in mean pyrite/(pyrite + pyrrhotite) from one zone to another are highly significant. For example, using Student's t test, it can be demonstrated that the difference in mean pyrite/(pyrite + pyrrhotite) between all rocks in the chlorite zone and all those in the sillimanite zone is significant at a >99.9% confidence level. Evidently some mineral reaction converts pyrite to pyrrhotite during progressive metamorphism. The conversion of pyrite to pyrrhotite by metamorphic reactions is, of course, also indicated by the observation that pyrite is abundant in marine black shales while pyrrhotite either occurs in trace amounts or is absent entirely.

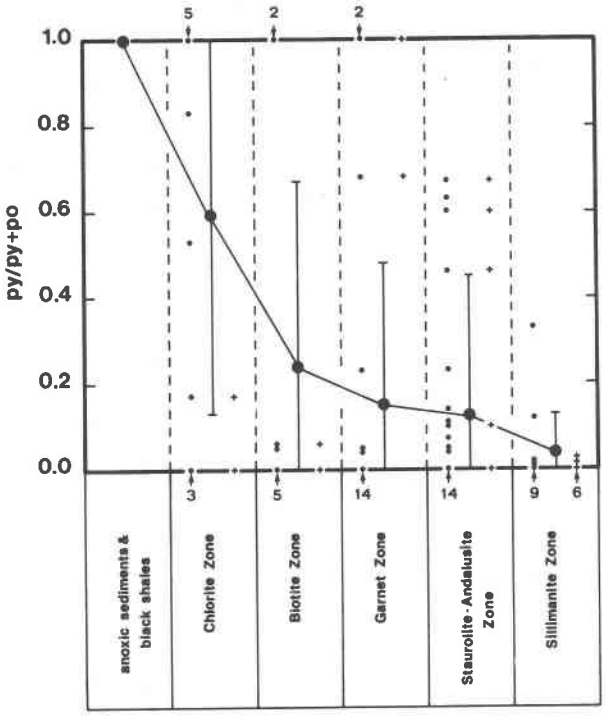

Fig. 3. Change in measured molar pyrite/ (pyrite + pyrrhotite) in schists as a function of increasing grade of metamorphism. Crosses are graphitic sulfide-rich schists from the study area. Small circles are normal pelitic schists and the graphitic sulfide-rich schists (combined) from the study area. Large circles represent the mean pyrite/(pyrite + pyrrhotite) of all samples within a metamorphic zone; vertical light line from circle to cross-bar represents one standard deviation about that mean. Small numbers identify the number of samples that plot at the same value of py/(py + po), if more than one.

The reaction that converts pyrite to pyrrhotite during metamorphism is unusual in two respects. First, the reaction is "smeared out" essentially over all

metamorphic grades: the quenched reaction is observed in at least some rocks from all metamorphic zones. Second, judging from data in Figure 3, the reaction has gone to completion in at least some samples from all metamorphic zones. Both observations suggest that increasing temperature is not the sole mechanism that drives the pyrite–pyrrhotite transition. Some phenomenon other than increasing temperature must be an important factor.

The pyrite–pyrrhotite reaction

Three possible types of mineral reactions could be responsible for the conversion of pyrite to pyrrhotite observed in rocks from the study area. One type involves the reaction of pyrite to pyrrhotite without loss or gain of either sulfur or iron from the rock. Such a reaction can be represented schematically as:

$$\underset{\text{pyrite}}{2\,FeS_2} + \underset{\text{oxide or silicate}}{2\,FeO} + \underset{\text{graphitic material}}{C} = \underset{\text{pyrrhotite}}{4\,FeS} + \underset{\text{fluid}}{CO_2} \quad (2)$$

Reactions of type 2 require that some element be oxidized to balance the reaction. Carbon was chosen for this role in reaction 2 because all graphitic sulfide-rich rocks contain abundant elemental carbon. Methane may also be oxidized in other reactions like 2. Other possible elements and species seem less likely to be involved in reactions like 2. Elemental hydrogen did occur in the metamorphic fluid (Table 6) but only in small concentrations. Iron as FeO could be oxidized to Fe_2O_3 but no minerals containing substantial amounts of ferric iron were observed in pyrrhotite-bearing rocks.

Regardless of which element is oxidized, there are three important consequences of reaction 2 that can be tested by data from rocks undergoing the pyrite–pyrrhotite reaction: (a) depending on the composition of pyrrhotites, approximately two moles of pyrrhotite form for every mole of pyrite consumed; (b) whole-rock sulfur and iron contents are unaffected by the reaction; and (c) as pyrrhotite forms, participating oxides and/or silicates decrease in modal abundance. If participating silicates are Fe–Mg solid solutions, the silicates become depleted in iron components. Reactions of type 2 have been proposed by Thompson (1972) and Robinson and Tracy (1976).

A second type of reaction converts pyrite to pyrrhotite at constant whole-rock sulfur content by adding iron to the rock. Such reactions can be represented schematically as:

$$\underset{\text{pyrite}}{2\,FeS_2} + \underset{\text{fluid}}{2\,FeCl_2 + 2\,H_2O} + \underset{\text{graphitic material}}{C} = \underset{\text{pyrrhotite}}{4\,FeS} + \underset{\text{fluid}}{4\,HCl + CO_2} \quad (3)$$

Consequences of reaction 3 are: (a) approximately two moles of pyrrhotite form for every mole of pyrite consumed: (b) whole-rock sulfur contents are unaffected by the reaction but whole-rock iron contents increase with reaction progress; and (c) as pyrrhotite forms, iron oxides and/or Fe–Mg silicates will be likely to increase in modal abundance through mineral–fluid reactions. Silicates that are Fe–Mg solid solutions will likely become enriched in iron components.

The third type of reaction converts pyrite to pyrrhotite at constant whole-rock iron content by desulfidation. Such a reaction can be represented schematically as:

$$\underset{\text{pyrite}}{2\,FeS_2} + \underset{\text{fluid}}{2\,H_2O} + \underset{\text{graphitic material}}{C} = \underset{\text{pyrrhotite}}{2\,FeS} + \underset{\text{fluid}}{2\,H_2S + CO_2} \quad (4)$$

Consequences of reaction 4 are: (a) approximately one mole of pyrrhotite forms for every mole of pyrite consumed; (b) whole-rock iron contents are unaffected by the reaction but whole-rock sulfur contents decrease as the reaction progresses; and (c) as pyrrhotite forms, oxides and/or silicates are unaffected in either their modal abundance or their composition.

Mineralogical, mineral chemical, and whole-rock chemical data on the graphitic sulfide-rich schists can be used to test for the most plausible reaction among types 2, 3, and 4. Selected mineralogical, mineral chemical, and whole-rock chemical parameters for all samples are plotted in Figures 4–7. Data in Figure 3 demonstrate that a pyrite–pyrrhotite reaction occurred in at least some rocks at all metamorphic grades. In plotting data from samples in all zones on the same diagram (Figs. 4–7), it is implicitly assumed that the pyrite–pyrrhotite transition occurs by the same reaction type in each zone regardless of metamorphic conditions. Such an assumption is justified for samples from the garnet, staurolite + andalusite, and sillimanite zones, because the rocks have very similar mineralogies. For samples in the three highest

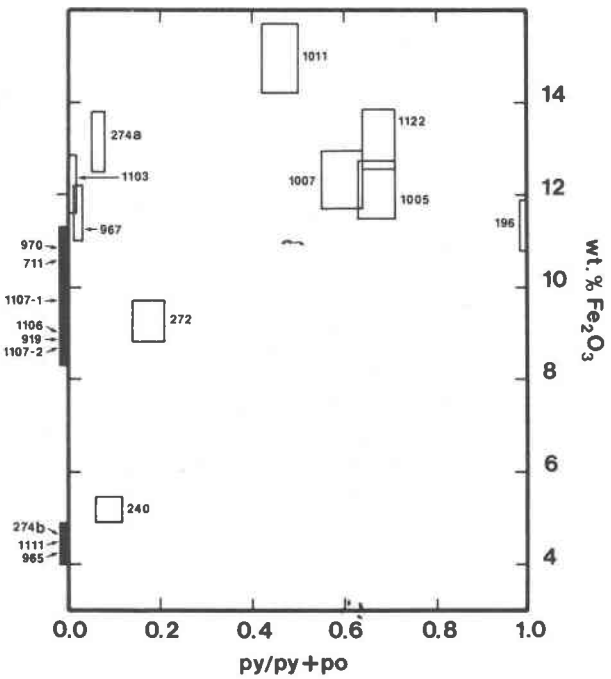

Fig. 4. Measured relationship between molar pyrite/(pyrite + pyrrhotite) and total whole-rock iron for the graphitic sulfide-rich schists. Sample numbers refer to Figure 1. Dimension of boxes represent ±5% relative error in the total iron value and two standard deviations of measured py/(py + po). Heavy line at left margin of diagram shows range in whole rock iron (considering a ±5% error) for pyrite-free rocks.

grade zones there is no suggestion that different reaction types are responsible for the pyrite–pyrrhotite transition in different zones. In Figures 4–7 reaction progress for the pyrite–pyrrhotite reaction is measured by the molar ratio of pyrite/(pyrite + pyrrhotite). For unreacted rocks the ratio is 1; for rocks in which the reaction has gone to completion, the ratio is 0.

Figure 4 is a plot of whole-rock iron content against reaction progress. There is no systematic relationship between these two variables. If any relation can be inferred to exist, it is a correlation of decreasing whole-rock iron contents with increasing reaction progress. Data in Figure 4 are consistent with reactions 2 or 4 but not with reaction 3.

Figure 5 shows molar whole-rock S/Fe against reaction progress. The advantage of monitoring whole-rock molar S/Fe is that it should change in a quantitatively predictable fashion depending on which type of reaction, 2, 3, or 4, occurred during metamorphism. If all iron in the unmetamorphosed equivalents of the graphitic sulfide-rich schists were combined with sulfur as pyrite (as was argued above) and if reactions 3 or 4 occurred, data points for pyrite-bearing samples should lie along an inclined line depending on the composition of pyrrhotite produced. The line marked "FeS" corresponds to a reaction like 3 or 4 that produces stoichiometric FeS. The line marked "$Fe_{0.9}S$" corresponds to a reaction like 3 or 4 that produces pyrrhotite with composition $Fe_{0.9}S$. If reactions like 2 occurred, then data points for pyrite-bearing samples should lie along the horizontal line labelled "constant sulfur and iron." There is a considerable scatter in the data points, and some of it reflects the practical difficulties in obtaining accurate chemical data on sulfur-rich rocks. As indicated by the long arrows, measured S/Fe values for samples 196A and 1007B are probably too low because the rocks contain some pyrite altered to limonite by surficial weathering. On the other hand, as indicated by the short arrow, measured S/Fe for sample 240A is probably slightly too high because

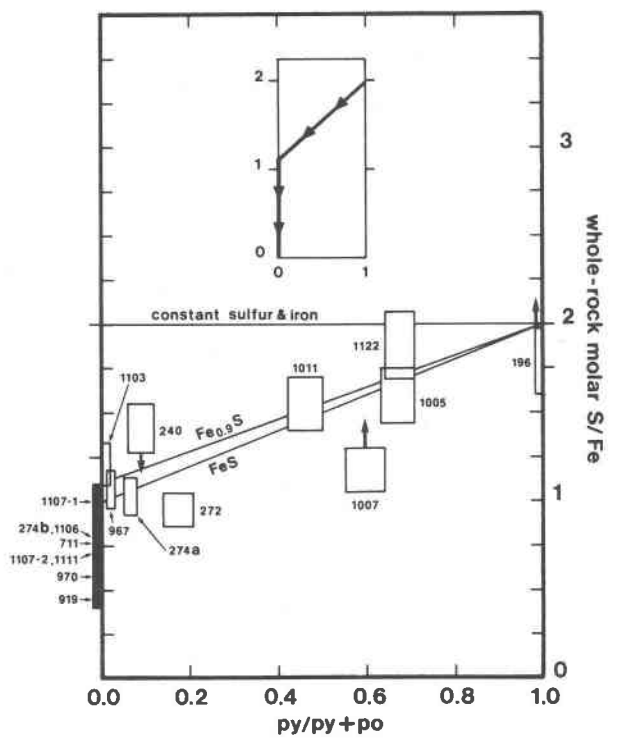

Fig. 5. Measured relationship between molar pyrite/(pyrite + pyrrhotite) and whole-rock molar S/Fe for the graphitic sulfide-rich schists. Sample numbers refer to Figure 1. Dimensions of boxes represent ±5% relative error in the total iron and sulfur values and two standard deviations of measured py/(py + po). Heavy line at left margin of diagram shows range in whole-rock S/Fe (considering ±5% errors) for pyrite-free rocks. Straight lines and inset explained in text.

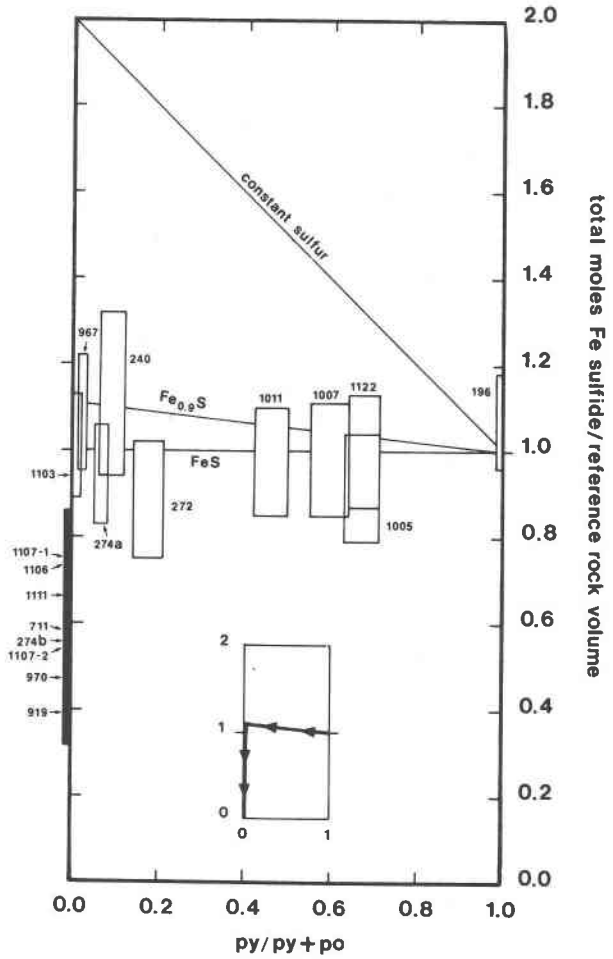

Fig. 6. Measured relationship between molar pyrite/(pyrite + pyrrhotite) and total moles pyrite + pyrrhotite for a reference volume of graphitic sulfide-rich schist. Sample numbers refer to Figure 1. Dimensions of boxes represent two standard deviations of the measured modal quantities and a ±5% relative error on total whole-rock iron values. Heavy line at left margin of diagram shows range in total moles pyrrhotite (considering appropriate errors) for a reference volume of pyrite-free rock. Straight lines and inset explained in text.

the rock contains a substantial amount of pyrrhotite altered to marcasite by surficial weathering. After the special considerations for samples 196A, 240A, and 1007B are taken into account, the data in Figure 5 are reasonably consistent with the hypothesis that the rocks initially contained all iron as pyrite and that pyrrhotite was produced by either reactions 3 or 4. The data in Figure 5 are inconsistent with a suite of rocks of similar initial bulk composition that were later affected by reaction 2. Data in Figure 4 document that there is no obvious systematic change of whole-rock iron content with reaction progress. The array of data points in Figure 5 for pyrite-bearing samples is interpreted, therefore, as evidence for a progressive loss in whole-rock sulfur with increasing progress of the pyrite → pyrrhotite reaction. The array of data points in Figure 5 for pyrite-free rocks results from mineral reactions unrelated to the pyrite–pyrrhotite transition and will be discussed below.

Figure 6 shows total moles of iron sulfide in all samples against reaction progress. Adopting the approach that Brimhall (1979) has used in a related problem, the total moles of iron sulfide were measured relative to a reference volume of rock that initially contained one mole of pyrite. The reference volume for each sample was determined in the following fashion. Sample 196A, the only graphitic sulfide-rich schist virtually free of pyrrhotite, contains 1 mole pyrite/165 cm^3 rock (Table 3). The sample also contains 0.1422 moles total iron/100 g rock. If, as was argued above, all iron in the unmetamorphosed equivalents to the schists resided in pyrite, then whole-rock iron serves as a measure of the original, premetamorphic pyrite content for each sample. Samples with iron contents greater than sample 196A contained one mole of pyrite in a rock volume less than 165 cm^3; samples with iron contents less than sample 196A contained one mole of pyrite in a rock volume greater than 165 cm^3. The quantitative rela-

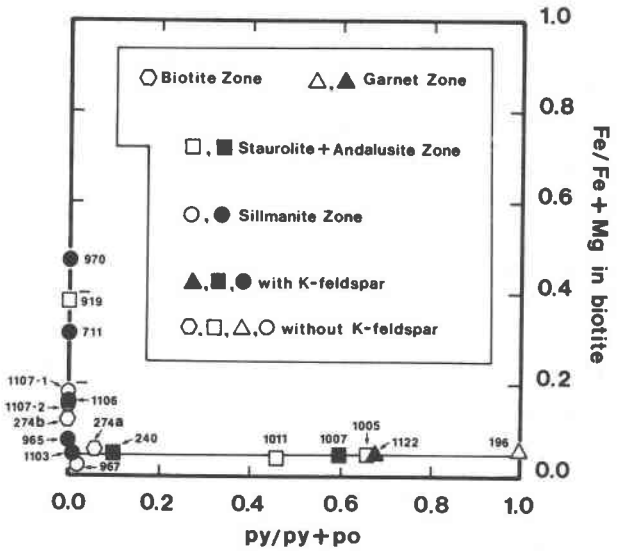

Fig. 7. Measured relationship between molar pyrite/(pyrite + pyrrhotite) and biotite composition for the graphitic sulfide-rich schists. Sample numbers refer to Figure 1. Horizontal line marks biotite composition of Fe/(Fe+Mg) = 0.045.

tionship between the reference volume (V_i) of any sample i, the reference volume of sample 196A, and the whole-rock iron content of the two samples is

$$V_i = \frac{(165\ \text{cm}^3)(0.1422\ \text{moles Fe/100 g sample 196A})}{(\text{X moles Fe/100 g sample i})} = \frac{F}{(\text{X moles Fe/100 g sample i})} \quad (5)$$

where X is determined from data in Table 5. The value for F actually may be in the range 21–26 based on errors in modal analysis and an assumed ±5% relative error in the iron content of sample 196A. Average F was rounded to the nearest value of 5 and F = 25 was chosen in the calculation of reference volumes. Equation 5 will predict the volume of rock that contained one mole of pyrite even if all iron initially did not reside in pyrite, providing that the *fraction* of whole-rock iron that resided in pyrite was the same for all samples prior to metamorphism.

If reactions like 4 occurred, then data points for pyrite-bearing samples should lie along a horizontal or near-horizontal line depending on the composition of pyrrhotite produced. The line marked "FeS" corresponds to a reaction like 4 that produces stoichiometric FeS. The line marked "$Fe_{0.9}S$" corresponds to a reaction like 4 that produces pyrrhotite with composition $Fe_{0.9}S$. If either a reaction like 2 or 3 occurred, data points for pyrite-bearing samples would lie along the inclined line. Total moles of sulfide are unchanged during the pyrite–pyrrhotite reaction in the reference volume of rock. Approximately one mole of pyrrhotite therefore is produced for every mole of pyrite consumed. The data are consistent with a suite of rocks that was affected by a reaction like 4 but not by reactions like 2 or 3. The array of data points in Figure 6 for pyrite-free rocks results from mineral reactions unrelated to the pyrite–pyrrhotite transition and will be discussed later.

Figure 7 shows the composition of biotite in the graphitic sulfide-rich schists against reaction progress. In all samples but 274A biotite occurs as the only Fe–Mg silicate. The only oxide mineral in these rocks is rutile. There is no relation between biotite composition and reaction progress for pyrite-bearing specimens. Because reactions like 2 and 3 predict changes in the composition of Fe–Mg silicates with reaction progress, data for pyrite-bearing samples in Figure 7 are inconsistent with reactions like 2 or 3. Data in Figure 7 are consistent with a reaction like (4) that does not affect the compositions of Fe–Mg silicates in rocks undergoing the pyrite-pyrrhotite transition. The lack of correlation between biotite composition and reaction progress is particularly important for those pyrite-bearing specimens represented by filled symbols in Figure 7. These rocks contain the assemblage biotite + K-feldspar + pyrite + pyrrhotite + graphitic material. A sulfide-silicate reaction is possible in these rocks such as

$$\underset{\text{biotite}}{2\,KFe_3AlSi_3O_{10}(OH)_2} + \underset{\text{pyrite}}{6\,FeS_2} + \underset{\text{graphitic material}}{3\,C} = \underset{\text{K-feldspar}}{2\,KAlSi_3O_8} + \underset{\text{pyrrhotite}}{12\,FeS} + \underset{\text{fluid}}{2\,H_2O + 3\,CO_2} \quad (2A)$$

There is no evidence, however, that a reaction like 2A took place in the pyrite-bearing samples. The array of data points in Figure 7 for pyrite-free rocks results from mineral reactions unrelated to the pyrite–pyrrhotite transition and will be discussed later.

Only desulfidation reactions like 4 are consistent with a pyrite–pyrrhotite transition and the data in Figures 4–7. Considering the major species in the metamorphic fluid (Table 6), it is likely that two desulfidation reactions occurred in the study area during metamorphism. At chlorite through staurolite + andalusite zone conditions, the pyrite–pyrrhotite transition probably dominantly occurred by

$$\underset{\text{pyrite}}{2\,FeS_2} + \underset{\text{fluid}}{CH_4} = \underset{\text{pyrrhotite}}{2\,FeS} + \underset{\text{fluid}}{2\,H_2S} + \underset{\text{graphitic material}}{C} \quad (4A)$$

In the sillimanite zone, fluids were CO_2–H_2O mixtures, and the pyrite–pyrrhotite transition probably dominantly occurred by reaction 4. Both reactions 4 and 4A, however, proceeded at least to some small degree at all metamorphic conditions.

Because reactions 4 and 4A involve elemental carbon, there should be a relationship between the reduced carbon content of pyrite-bearing rocks and progress of the pyrite–pyrrhotite reaction. Examination of the data in Table 5 reveals that no such systematic relationship exists. Several explanations are possible. First, for carbonate-bearing samples, total carbon reported in Table 5 is not equivalent to reduced carbon. Second, desulfidation reaction 4 consumes carbon while reaction 4A produces it. Consequently the two reactions will affect the reduced carbon content of rocks in opposite ways. Third, a

systematic relationship between reduced carbon content and reaction progress is expected only for suites of pyrite-bearing rocks undergoing the same reaction and with the same pre-metamorphic contents of elemental carbon. Chemical analyses of black shales (Pettijohn, 1975) indicate that this would be an unlikely circumstance. Unlike the case for pyrite, there is no obvious way to estimate a reference volume of graphitic sulfide-rich schist that initially contained one mole of reduced carbon prior to metamorphism.

Because reactions like 2 have been invoked to explain the pyrite–pyrrhotite transition in pelitic schists (Thompson, 1972; Robinson and Tracy, 1976), it is worthwhile to mention additional arguments why reaction 2 is unlikely to be responsible for the pyrite-pyrrhotite transition in the study area. First, observations about pyritic black shales seem to indicate that reactions like 2 could not proceed to a significant degree during metamorphism. Black shales contain pyrite and either only trace amounts of pyrrhotite or, as is more common, no pyrrhotite at all. All or almost all iron (85–100%) in the black shales is bound in pyrite. Reactions like 2 convert pyrite to pyrrhotite by extraction of iron from oxides and/or silicates and combining it with pyrite. Consequently, if all the pyrite is converted to pyrrhotite by a reaction such as 2, at least 40–50 mole percent iron in a rock must reside in oxides and/or silicates prior to metamorphism. Data on pyritic black shales indicate that there simply is not sufficient iron in silicates or oxides in these rocks for reaction 2 to be quantitatively effective. Samples of graphitic sulfide-rich schist illustrate, as well, the problem of insufficient iron in silicates. Modal data in Table 3 and mineral composition data in Tables 2 and 4 can be used to estimate the total amount of iron in silicates in rocks 1007B, 1011A, and 1122 G, which is 0.153, 0.146, and 0.193 moles Fe/1000 cm^3 rock, respectively. The rocks contain 3.57, 3.36, and 4.45 moles pyrite/1000 cm^3 rock respectively (Table 3). Even if *all* iron in the silicates in the three rocks had been used to convert pyrite to pyrrhotite by reactions like 2, only 4–5% of the pyrite would have been consumed. A proponent of reaction 2 could argue that the low iron content of the silicates in the three samples prevented the conversion of pyrite to pyrrhotite. The mineralogy of the graphitic sulfide-rich schists from the sillimanite zone, however, suggests that the pyrite–pyrrhotite transition is essentially completed in all rocks at least at high grades. If the low iron content of silicates can prohibit completion of the pyrite–pyrrhotite reaction, then it is surprising that not one sample of graphitic sulfide-rich schist from the sillimanite zone contains more than 0.3 modal percent pyrite while in each of the lower grade zones one or more samples contain 1.0–14.5 modal percent pyrite.

Second, if reactions like 2 are to occur, some reaction relationship between sulfides and silicates must exist in the rocks. Such a reaction relation is missing in many pyrite-bearing samples. For example, specimen 1011A contains, as major minerals, pyrite + pyrrhotite + biotite + plagioclase + quartz. No reaction can be written between components of the sulfide minerals and the silicates. Added consideration of the accessory phases does not reveal any reaction relationship among sulfides, major minerals, and accessory minerals. A proponent of reactions like 2 might argue that the lack of a sulfide–silicate reaction relationship in specimens like 1011A is what preserves pyrite in the rock. If this were true, however, it is surprising that all samples of schist collected in the sillimanite zone show evidence of an essentially complete pyrite–pyrrhotite reaction. Using a similar argument as above, if reaction could be limited by lack of a sulfide–silicate reaction relation, it is difficult to understand why not one sample of sillimanite zone schist contains more than a trace of pyrite.

Third, graphic analysis of the pyrite–pyrrhotite transition seems to favor a reaction like 4 rather than a reaction such as 2. Figure 2 illustrates the composition of coexisting sulfides and biotite in the assemblage biotite + K-feldspar + graphitic material + pyrrhotite ± pyrite. Compositions of minerals are related by reaction relation 2A, and pyrrhotite could conceivably have been produced through this reaction. Graphically the effects of hypothetical reaction 2A are illustrated in Figures 2b and 2c. If reaction 2A were to occur with increasing grade, the biotite–pyrite–pyrrhotite triangle would sweep to the right in the diagram. As reaction proceeds and the triangle sweeps to the right: (a) pyrite-bearing rocks (composition A) develop pyrrhotite; (b) the ratio pyrite/(pyrite + pyrrhotite) decreases in rocks with pyrite + pyrrhotite but rich in pyrite (composition B); and (c) rocks with pyrite + pyrrhotite but rich in pyrrhotite (composition C) lose pyrite. The actual data from the graphitic sulfide-rich schists (Fig. 2a) might be interpreted as a state reached after the three-phase triangle swept across the diagram to the composition of biotite at Fe/(Fe+Mg) = 0.047. The principal argument against such an interpretation is that there is no evidence that the biotite–pyrite–pyrrhotite triangle ever swept across the diagram. All samples with pyrite + pyrrhotite + K-feldspar + graphitic material

contain biotite with essentially the same Fe/(Fe+Mg) = 0.046–0.048. The samples were collected from metamorphic grades ranging from garnet through sillimanite zone conditions. If the three-phase triangle did indeed sweep across the diagram in Figure 2 it is surprising that not one sample "catches" the triangle in a position other than at Fe/(Fe+Mg) = 0.047. It seems fortuitous that the sweep of the triangle would have stopped at the same biotite composition in all samples from three different metamorphic zones. There is no evidence that the biotite–pyrite–pyrrhotite triangle ever was in a position other than Fe/(Fe+Mg) = 0.047 during metamorphism of the graphitic sulfide-rich schists. I conclude that the triangle always was positioned at Fe/(Fe+Mg) = 0.047±0.001 and that reaction 2A never occurred in the rocks.

I attribute the regular array of tie lines and mineral compositions in Figure 2a to a close approach to chemical equilibrium among a suite of samples that differ in bulk composition. Samples that plot to the left in the diagram have lower molar S/Fe relative to samples that plot in the righthand portion of the diagram. What is the cause of the variation in bulk rock composition? The difference in bulk composition among the samples could reflect differences in pre-metamorphic rock composition acquired during sedimentation and/or diagenesis. If this were true, then natural processes have provided remarkable demonstration of foresight. Dotted vertical lines in Figure 2a segregate the samples by metamorphic zone. The samples lowest in molar S/Fe were collected in the sillimanite zone. The sample highest in S/Fe was collected in the garnet zone. Samples of intermediate S/Fe were collected in the intervening staurolite + andalusite zone. If the S/Fe of the metamorphic rocks were entirely controlled by sedimentation and diagenesis, then sedimentary and diagenetic processes were apparently able to deposit low S/Fe rocks with perfect accuracy precisely where later high grade metamorphism was to occur. Sedimentary and diagenetic processes were apparently also able to deposit high S/Fe rocks only where later low grade metamorphism would occur. I adopt an interpretation of the array of data points in Figure 2a that involves less coincidence. If rocks experience desulfidation during metamorphism, high grade rocks will, on the average, have lower S/Fe than lower grade rocks. Progressive metamorphism of a suite of rocks, initially of similar bulk composition, will produce a suite of metamorphic rocks with variable S/Fe that will plot in a subhorizontal array across Figure 2a. High grade rocks will plot further to the left in the array; lower grade rocks will plot to the right. I interpret the range in bulk rock compositions illustrated in Figure 2a as caused by desulfidation during metamorphism. The graphical analysis of the graphitic sulfide-rich schists requires that if pyrrhotite formed by reaction 2A, then an implausible number of fortuitous events occurred. The graphical analysis is consistent, on the other hand, with development of pyrrhotite in the graphitic sulfide-rich schists by desulfidation reactions such as 4 and 4A.

Sulfide–silicate relations

Mineral reactions between sulfides and silicates may explain some of the compositions of silicate minerals observed in the graphitic sulfide-rich schists.

Composition of biotite coexisting with pyrite + pyrrhotite

A striking aspect of the mineral composition data in Figure 7 is the regular relationship between biotite composition and the assemblage of iron sulfides in the graphitic sulfide-rich schists. In rocks containing pyrite + pyrrhotite, Fe/(Fe+Mg) of biotite is 0.018–0.056. For rocks containing pyrite + pyrrhotite + K-feldspar, the biotite is even further restricted in composition, Fe/(Fe+Mg) = 0.046–0.048. All rocks without pyrite contain biotite with Fe/(Fe+Mg) = 0.075–0.467. The composition of biotite coexisting with pyrite + pyrrhotite is fixed over the entire range of metamorphic conditions from the biotite through sillimanite zones. Furthermore, the relationship appears to be a general one: Robinson and Tracy (1976) report that Fe/(Fe+Mg) of biotite in pyrite + pyrrhotite-bearing schists from a sillimanite + K-feldspar zone in central Massachusetts has nearly the same value, 0.05.

The unique composition of biotite coexisting with pyrite + pyrrhotite in biotite zone rocks may be a consequence of a low variance mineral assemblage that existed in the graphitic sulfide-rich rocks when biotite first formed. Pyrite-bearing phyllites of the chlorite zone contain dolomite + muscovite + albite + quartz + rutile + graphitic material + chalcopyrite + pyrite + pyrrhotite ± calcite. At higher grades, pyrite-bearing schists contain biotite + plagioclase ($X_{an} > 0.3$) + quartz + rutile + graphitic material + chalcopyrite + pyrite + pyrrhotite ± K-feldspar ± muscovite ± chlorite ± siderite. Only two samples were collected from the biotite zone, and neither of them appears to contain a complete record of what miner-

als were involved in the reaction that formed biotite. By combining the assemblages found in chlorite zone rocks with those in higher grade rocks, the probable mineral assemblage that existed when biotite first crystallized may be estimated: muscovite + dolomite + biotite + albite + oligoclase + quartz + rutile + graphitic material + chalcopyrite + pyrite + pyrrhotite ± K-feldspar ± chlorite ± calcite ± siderite. Coexisting albite and oligoclase are included because of the peristerite gap in the plagioclase solid solution series and because coexisting albite (An_{01}) and oligoclase (An_{24}) have been observed in normal pelitic schists from the biotite zone in the area of Figure 1 (Ferry, unpublished data). Compositions of minerals in the combined mineral assemblage can be expressed by the components K_2O, Na_2O, CaO, FeO, MgO, CuO, TiO_2, SiO_2, Al_2O_3, C, O, H, and S. MnO was not included because it occurs in concentrations of less than 0.3 weight percent in minerals from rocks collected within the chlorite, biotite, and garnet zones. In the presence of a C–O–H–S–Cl fluid of constant chloride concentration, at a given temperature and pressure, the assemblage muscovite + dolomite + biotite + albite + oligoclase + quartz + rutile + graphitic material + chalcopyrite + pyrite + pyrrhotite is univariant. If one of the four phases, chlorite, K-feldspar, calcite, or siderite is added, the assemblage is invariant. If MnO and Cl are considered as chemical variables, participation of any other two of the minerals, chlorite, K-feldspar, calcite, or siderite, would preserve the invariant state. It seems likely that the graphitic sulfide-rich rocks were a chemical system of very low variance, possibly invariant, when biotite first crystallized. If the system were invariant, the composition of all phases would be fixed, and the unique composition of biotite in rocks containing pyrite + pyrrhotite could be explained.

The exact reaction that formed biotite cannot be specified with great confidence. If K-feldspar is involved, a speculation that uses actual compositions of minerals in rocks of the biotite and chlorite zones (Table 7) and major species in the fluid phase (Table 6), might be

$$2.689 \text{ muscovite} + 4.648 \text{ albite} + 1.990 \text{ quartz} + 1.567 \text{ dolomite} + 0.029 \text{ pyrrhotite} + 0.030 \text{ rutile} + 3.139\ CH_4 = 1.000 \text{ biotite} + 6.269 \text{ oligoclase} + 1.600 \text{ K-feldspar} + 6.273\ C + 0.029\ H_2S + 7.937\ H_2O \quad (6)$$

The composition of the fluid and mineral solid solutions would all be fixed at a given pressure, temperature, and chloride content of fluid by the additional presence of pyrite.

Table 7. Typical compositions of minerals from graphitic sulfide-rich schists collected in the biotite and chlorite zones.

Mineral	Formula
muscovite	$K_{0.9}Na_{0.05}Mg_{0.3}Al_{2.35}Si_{3.35}O_{10}(OH)_2$
biotite	$K_{0.9}Fe_{0.12}Mg_{2.28}Ti_{0.03}Al_{1.53}Si_{2.90}O_{10}(OH)_2$
dolomite	$CaFe_{0.06}Mg_{0.94}(CO_3)_2$
pyrrhotite	$Fe_{0.9}S$
albite	$NaAlSi_3O_8$
oligoclase	$Ca_{0.25}Na_{0.75}Al_{1.25}Si_{2.75}O_8$
K-feldspar	$K_{0.95}Na_{0.05}AlSi_3O_8$
pyrite	FeS_2
quartz	SiO_2
rutile	TiO_2
graphitic material	C

At grades higher than the biotite zone, biotite is the only Fe–Mg mineral that occurs in major abundance (>2%) in the graphitic sulfide-rich schists. The observation suggests that the unique composition of biotite, coexisting with pyrite and pyrrhotite, was established in rocks when biotite first crystallized during biotite-zone conditions. The unique composition of biotite preserved in pyrite + pyrrhotite-bearing rocks may reflect that biotite subsequently never participated in any other mineral reactions when the rock was subjected to higher-grade metamorphic conditions.

Composition of biotite in pyrite-free rocks

The composition of biotite in rocks without pyrite is more iron-rich than Fe/(Fe+Mg) = 0.05. After pyrite is eliminated from the graphitic sulfide-rich schists by desulfidation reactions 4 and 4A, the more iron-rich biotites can be produced by continued desulfidation of rock by a mineral reaction such as 7:

$$\underset{\text{K-feldspar}}{KAlSi_3O_8} + 3\ \underset{\text{pyrrhotite}}{FeS} + 4\ \underset{\text{fluid}}{H_2O} = \underset{\text{biotite}}{KFe_3AlSi_3O_{10}(OH)_2} + 3\ \underset{\text{fluid}}{H_2S} \quad (7)$$

The K-feldspar involved in reaction 7 first appears in rocks collected from the garnet zone although the reaction by which it forms cannot be precisely specified from the few samples collected (reaction 6 is a possibility). Varying degrees of desulfidation would result in varying degrees of progress of reaction 7 and consequently in the range of biotite compositions in Fig-

ure 7. Half of the pyrite-free rocks plotted in Figure 7 do not contain K-feldspar. In these samples either the K-feldspar was completely consumed by desulfidation reaction 7 or the rocks never contained K-feldspar. If the rocks never contained K-feldspar, then the composition of biotite in them must be explained by some other mineral reaction. There is insufficient evidence, however, to speculate what these other mineral reactions may have been. Some of the pyrite-free rocks plotted in Figure 7, of course, *may* have not contained pyrite when biotite first crystallized in them. Such a situation could arise, as for sample 1111A, if the pyrite–pyrrhotite transition was completed in a specimen under metamorphic conditions of the chlorite zone. The composition of biotite in these rocks may therefore be a relict of some biotite-forming reaction in pyrite-free rocks. It would be impossible, however, to identify such rocks because there is no obvious way to tell at what point in the metamorphic evolution of a particular high-grade rock that pyrite was consumed.

Fluid-rock ratios during metamorphism

If the above analysis of the graphitic sulfide-rich schists is correct, pyrite + pyrrhotite-bearing rocks principally experienced reactions 4 and 4A during progressive metamorphism at garnet zone conditions and at higher grades. Reaction 4 produces fluid with composition $X_{H_2S} = 0.67$; $X_{CO_2} = 0.33$. Reaction 4A produces a pure H_2S fluid. There exists a large discrepancy between the composition of fluid generated by reactions 4 and 4A and the composition of CO_2–H_2O–CH_4 fluid with which the graphitic sulfide-rich rocks were in equilibrium (Table 6). This discrepancy in fluid compositions may be resolved using arguments developed previously from the study of metamorphosed carbonate rocks (Ferry, 1980a; Rumble *et al.,* 1981). The graphitic sulfide-rich schists probably equilibrated during metamorphism with a fluid mixture. One component of the fluid was rich in H_2S and was generated internally within the rocks by reaction 4 and 4A. The other component of the fluid originated from (unknown) sources external to the graphitic sulfide-rich schists. The externally-derived component was probably rich in those species that are consumed by reactions 4 and 4A as well as those species present in the equilibrium fluid but not produced by reactions 4 and 4A (*e.g.,* H_2O and CH_4). Judging from the compositions of the fluid mixtures with which the rocks equilibrated (Table 6) the mixtures were primarily composed of the externally-derived component with only small admixtures of the internally-generated, H_2S-rich component.

If some assumptions are made, the amount of externally-derived component that interacted with a rock specimen during the metamorphic event can be quantitatively estimated (*cf.* Ferry, 1980a). First, it will be assumed that the externally-derived fluid component contained no H_2S (and hence no total sulfur) prior to mixing with the fluid component generated by reactions 4 and 4A. This assumption is a "conservative" action because it leads to minimum estimates of the amount of the externally-derived fluid component. The assumption is justified by the very low sulfur content of fluids that were in equilibrium during metamorphism with other common rock types in the study area (Ferry, 1976; 1979). Let ξ represent a measure of progress for reaction 4 or 4A, where

$$\xi = \tfrac{1}{2} \text{ (moles pyrrhotite/1000 cm}^3 \text{ metamorphosed rock)} \quad (7)$$

The variable ξ is a simple measure of fluid species produced or consumed by reactions 4 and 4A. The value of ξ is equivalent to (a) half the number of moles H_2S produced by reaction 4 and 4A; (b) half the number of moles H_2O consumed by reaction 4; (c) the number of moles CO_2 produced by reaction 4; and (d) the number of moles CH_4 consumed by reaction 4A. The composition of metamorphic fluid in equilibrium with the sulfide-rich rocks is related to ξ and to the number of moles of the externally-derived fluid component, N, by the following relation:

$$X_{H_2S} = 2\,\xi/(N + \xi) \quad (8)$$

Values of ξ and X_{H_2S} can be derived from data in Tables 3 and 6, and N may be calculated from equation 8. If some assumption is made about the composition of the externally-derived fluid component, then N moles fluid can be converted to a certain volume of fluid. A second assumption made in calculating fluid–rock ratios during metamorphism is that the externally-derived fluid component had the same proportions of $H_2O : CH_4 : CO_2$ as the fluid in equilibrium with the schists. Such an assumption seems reasonable because the small X_{H_2S} contents of the equilibrium fluid require that the equilibrium fluid be dominantly composed of the externally-derived component. Consequently the equilibrium fluids should have compositions close to the composition of the externally-derived fluid component. Moles of fluid were converted to volume of fluid using molar volumes of H_2O from Burnham *et al.* (1969) and mo-

lar volumes of CO_2 from Shmonov and Shmulovich (1974). Molar volumes of CH_4 were derived from the fugacity coefficients of Ryzhenko and Volkov (1971) using the following relation:

$$(\partial \ln f_{CH_4}/\partial P)_T = \overline{V}_{CH_4}/RT \quad (9)$$

Components were assumed to mix ideally with respect to volume in the fluid.

Fluid-rock ratios calculated for samples for which there are data on equilibrium fluid compositions are presented in Table 8. Documentation that desulfidation reactions like 4 and 4A occurred during metamorphism is significant because it demonstrates that very large volumes of externally-derived fluid interacted with the rocks during metamorphism (fluid–rocks ratios > 1 on a volume basis). Results reported in Table 8 are in harmony with recent investigations of the volumes of fluid that interact with carbonate rocks during metamorphism (Ferry 1980a; Bowman *et al.*, 1980; Rumble *et al.*, 1981)

Table 8. Volume of externally-derived C–O–H fluid that interacted with a reference volume of 1000 cm³ graphitic sulfide-rich schist during metamorphism. Extensive quantities refer to 1000 cm³ metamorphosed rock

Specimen Number	moles of pyrrhotite	ξ	moles fluid	volume of fluid (cm³)	volumetric fluid/rock
1122G	2.10	1.050	138.95	5004	5.0
1007B	2.43	1.215	72.42	2375	2.4
240A	2.66	1.330	70.56	2226	2.2
1103-1	6.10	3.050	118.85	3501	3.5

A model for desulfidation during metamorphism

The following sequence of events is envisioned during the metamorphic evolution of the graphitic sulfide-rich schists. At the end of diagenesis the rocks contain pyrite, dolomite, muscovite, albite, graphitic material, and a variety of accessory minerals. Essentially all iron in the rocks is combined with sulfur as pyrite. Grain boundaries are wetted, probably by H_2O and CH_4. As temperature increases during metamorphism, small amounts of pyrrhotite will form dominantly by reaction 4A. Reaction will cease, however, as soon as the amount of H_2S, released by desulfidation, accumulates along grain boundaries in concentrations that equal those for a fluid in equilibrium with pyrite + pyrrhotite + carbon. For further reaction to occur, the accumulated H_2S must be removed from the rock. It is envisioned that the H_2S is flushed out by an aliquot of H_2O–CH_4–CO_2 fluid derived from (unknown) sources external to the sulfide-rich schists and very low in total sulfur content. The externally-derived fluid is believed to flow through the sulfide-rich rocks in response to either small, local pressure gradients or buoyancy forces. Once the initially-produced H_2S has been flushed out by the externally-derived fluid, a new increment of reaction 4A occurs. Actually reaction and fluid flow probably did not take place in discrete steps but in one continuous process. The flow of externally-derived fluid is sufficiently slow that minerals in the rock are able to buffer, through mineral–fluid reactions, the composition of fluid occupying the pore space of the schists at any one instant. The constant influx of externally-derived fluid, initially out of equilibrium with the sulfide-rich rocks, is however, an essential driving force behind the desulfidation reaction. Because the influx of externally-derived fluid drives the desulfidation reaction, the reaction is not exclusively dependent upon increasing temperature and may occur at any metamorphic grade. Consequently desulfidation reactions 4 and 4A are observed to go to completion in some samples in all metamorphic zones.

At some point, as temperature continues to rise during metamorphism, mineral reactions occur in the graphitic sulfide-rich schists, that produce biotite and K-feldspar at the expense of dolomite, muscovite, and other minerals. In pyrite-bearing rocks, the reaction involves an assemblage of very low variance and consequently biotite of only a very restricted compositional range forms. Continued influx of externally-derived fluid drives desulfidation reaction 4A, causing the ratio pyrite/(pyrite + pyrrhotite) in the rocks to decrease and depleting the rock of sulfur. In some rocks pyrite is completely converted to pyrrhotite. Further infiltration of the externally-derived fluid causes additional desulfidation by driving reaction 7 in rocks with K-feldspar. As reaction 7 progresses, biotite in the rock becomes progressively enriched in iron components. Desulfidation of pyrrhotite-bearing rocks by reaction 7 proceeds either until one of the mineral reactants is exhausted (*e.g.*, K-feldspar) or until the metamorphic event terminates.

When temperatures have reached those characteristic of sillimanite zone conditions, desulfidation of pyrite-bearing rocks occurs dominantly by reaction 4 rather than 4A. Very few sulfide-rich schists retain pyrite. Most schists contain only pyrrhotite and with increasingly iron-rich biotite. Fluid–rock ratios in Table 8 are an approximate measure of the volume of externally-derived fluid that has flowed through the schists as desulfidation occurred during the entire metamorphic event.

The model of desulfidation predicts how the S/Fe molar whole-rock ratio should change in all graphitic

sulfide-rich rocks as a function of sulfide mineralogy. The prediction is illustrated in the inset to Figure 5 by the heavy line. Arrows point in the direction of changes produced by progressive desulfidation. The inclined portion of the heavy line reflects the effects of reactions 4 and 4A; the vertical portion of the line reflects the effects of reaction 7. Data points for pyrrhotite-bearing rocks with and without pyrite closely fit the expected trends. The model of desulfidation also predicts how the total number of moles of iron sulfide per reference volume of rock should change in all graphitic sulfide-rich rocks as a function of sulfide mineralogy. The prediction is illustrated in the inset to Figure 6 by the heavy line. Arrows again point in the direction of changes produced by progressive desulfidation. The subhorizontal portion of the heavy line reflects the effects of reactions 4 and 4A; the vertical portion of the line reflects the effects of reaction 7. Data points for the sulfide-rich schists closely fit expected trends. The data points in Figure 7 also are consistent with the model for desulfidation. The horizontal array of data points for pyrite-bearing rocks reflects that desulfidation of pyrite-bearing rocks does not involve sulfide–silicate reactions. The vertical array of data points for pyrite-free rocks reflects the effect of reaction 7 on biotite composition.

Types of externally-derived fluids

The model for desulfidation presented above is very similar to a model for decarbonation during metamorphism proposed by Rumble *et al.* (1981). The principal difference between the desulfidation and decarbonation models is the composition of the externally-derived fluids. Mineral equilibria in the graphitic sulfide-rich schists suggest that the externally-derived fluids were H_2O–CH_4–CO_2 mixtures. Mineral equilibria in calc-silicate rocks suggest that the externally-derived fluid was essentially pure H_2O. This compositional difference appears to correlate with the difference in composition of fluid inclusions found in calc-silicate rocks and in graphitic schists. Fluid inclusions found in calc-silicate rocks are either nearly pure H_2O or aqueous brines (Crawford *et al.*, 1979; Kreulen, 1980). Neither pure H_2O nor aqueous brines are produced by common decarbonation reactions in calc-silicate rocks. The fluid in the inclusions may represent trapped samples of externally-derived fluid. CO_2–H_2O–CH_4 fluids with various compositions have been observed as inclusions in schists and semi-pelitic rocks (Crawford *et al.*, 1979; Hollister and Burruss, 1976; Kreulen, 1980). CO_2–H_2O–CH_4 fluids are not produced by common dehydration reactions in metapelitic rocks. The fluid inclusions in pelitic rocks may represent trapped samples of externally-derived fluid.

Petrologic studies and studies of fluid inclusions are consistent with at least two types of externally-derived fluid. One is H_2O-rich and associated with calc-silicate rocks while the other is a CO_2–H_2O–CH_4 mixture and is associated with graphitic metashales. The two types of externally-derived fluid appear to occur together in at least some terrains. In the study area of Figure 1 graphitic sulfide-rich schists interacted during metamorphism with externally-derived CO_2–H_2O–CH_4 fluids (this study) while calc-silicate rocks interacted with externally-derived H_2O fluid (Ferry, 1980a). At Naxos some calc-silicate horizons contain inclusions of nearly pure H_2O while schists, quartzites, and marbles contain inclusions of pure CO_2 (Kreulen, 1980). In the Prince Rupert area, British Columbia, calc-silicates include aqueous brines, while semi-pelitic rocks contain inclusions of CO_2–CH_4 mixtures. These observations suggest a highly channelized and complicated mechanism of fluid transfer during metamorphism.

The origin of the two types of externally-derived fluid is not known. The fluids could be products of metamorphic devolatilization reactions. Some externally-derived fluid, however, may originate in the mantle. Externally-derived H_2O could conceivably represent seawater/meteoritic water that has penetrated deep into the crust. The origin of the externally-derived fluids may be revealed by multidisciplinary studies involving mineral equilibria, fluid inclusions, and stable isotopes.

Acknowledgments

Research was supported by a Cottrell Grant from Research Corporation and NSF grants EAR 77-22771 and 80-20567 (Earth Sciences Section). Electron microprobe analyses were obtained at the Geophysical Laboratory with the kind permission of H. S. Yoder, Jr., Director. Thanks are due to C. F. Lewis for performing whole-rock sulfur and carbon analyses. C. V. Guidotti, M. J. Holdaway, C. Klein, and R. P. Wintsch are warmly thanked for reviews that led to substantial improvements in an early version of the manuscript.

References

Albee, A. L. and Ray, L. (1980) Correction factors for electron probe microanalysis of silicates, oxides, carbonates, phosphates, and sulfates. Analytical Chemistry, 42, 1408–1414.

Barker, D. S. (1964) The Hallowell granite, south-central Maine. American Journal of Science, 262, 592–613.

Bates, T. F. and Strahl, E. O. (1957) Mineralogy, petrography, and radioactivity of representative samples of Chattanooga Shale. Geological Society of America Bulletin, 68, 1305–1315.

Bence, A. E. and Albee, A. L. (1968) Empirical correction factors of the electron microanalysis of silicates and oxides. Journal of Geology, 76, 382–403.

Berner, R. A. (1964) Distribution and diagenesis of sulfur in some sediments from the Gulf of California. Marine Geology, 1, 117–140.

Berner, R. A. (1970) Sedimentary pyrite formation. American Journal of Science, 268, 1–23.

Berner, R. A., Baldwin, T., and Holdren, G. R., Jr. (1979) Authigenic iron sulfides as paleosalinity indicators. Journal of Sedimentary Petrology, 49, 1345–1350.

Bowman, J. R., Essence, E. J., and O'Neil, J. R. (1980) Origins and evolution of metamorphic fluids in dolomitic marbles, Elkhorn, Montana. Transactions, American Geophysical Union, 61, 391.

Brimhall, G. H., Jr. (1979) Lithologic determination of mass transfer mechanisms of multiple-stage porphyry copper mineralization at Butte, Montana: vein formation by hypogene leaching and enrichment of potassium-silicate protore. Economic Geology, 74, 556–589.

Burnham, C. W., Holloway, J. R., and Davis, N. F. (1969) Thermodynamic properties of water to 1000°C and 10,000 bars. Geological Society of America Special Paper 132.

Carpenter, R. H. (1974) Pyrrhotite isograd in southeastern Tennessee and southwestern North Carolina. Geological Society of America Bulletin, 85, 451–456.

Colby, J. W. (1971) MAGIC IV, a computer program for quantitative electron microprobe analysis. Bell Telephone Laboratories, Allentown, Pennsylvania.

Conant, L. C. and Swanson, V. E. (1916) Chattanooga Shale and related rocks of central Tennessee and nearby areas. U.S. Geological Survey Professional Paper 357.

Crawford, M. L., Kraus, D. L., and Hollister, L. S. (1979) Petrologic and fluid inclusion study of calc-silicate rocks, Prince Rupert, British Columbia. American Journal of Science, 279, 1135–1159.

Dallmeyer, R. D. (1979) Chronology of igneous and metamorphic activity in south-central Maine. In Osberg, P. H. and Skehan, J. W., Editors, The Calendonides in the U.S.A., p. 63–72. Weston Observatory of Boston College, Weston, Massachusetts.

Elverhøi, A. (1977) Origin of framboidal pyrite in clayey Holocene sediments and in Jurassic black shale in the northwestern part of the Barents Sea. Sedimentology, 24, 591–595.

Erd, R. C., Evans, H. T., Jr. and Richter, D. H. (1957) Smythite, a new iron sulfide, and associated pyrrhotite from Indiana. American Mineralogist, 42, 309–333.

Eugster, H. P., and Skippen, G. B. (1967) Igneous and metamorphic reactions involving gas equilibria. In Abelson, P. H., Editor, Researches in Geochemistry, Volume II, p. 492–521. John Wiley and Sons, New York.

Ferry, J. M. (1976a) Metamorphism of calcareous sediments in the Waterville-Vassalboro area, south-central Maine: mineral reactions and graphical analysis. American Journal of Science, 276, 841–882.

Ferry, J. M. (1976b) P, T, f_{CO_2}, and f_{H_2O} during metamorphism of calcareous sediments in the Waterville–Vassalboro area, south-central Maine. Contributions to Mineralogy and Petrology, 57, 119–143.

Ferry, J. M. (1978) Fluid interaction between granite and sediment during metamorphism, south-central Maine. American Journal of Science, 278, 1025–1056.

Ferry, J. M. (1979) A map of chemical potential differences within an outcrop. American Mineralogist, 64, 966–985.

Ferry, J. M. (1980a) A case study of the amount and distribution of heat and fluid during metamorphism. Contributions to Mineralogy and Petrology, 71, 373–385.

Ferry, J. M. (1980b) A comparative study of geothermometers and geobarometers in pelitic schists from south-central Maine. American Mineralogist, 65, 720–732.

Ferry, J. M. (1980c) Extraction of alkali metals from argillaceous carbonate rocks during prograde regional metamorphism, south-central Maine. Geological Society of America Abstracts with Programs, 12, 425.

French, B. M. (1968) Progressive contact metamorphism of the Biwabik Iron-formation, Mesabi Range, Minnesota. Minnesota Geological Survey Bulletin 45.

Fullagar, P. D., Brown, H. S., and Hagner, A. F. (1967) Geochemistry of wall-rock alteration and the role of sulfurization in the formation of the Ore Knob sulfide deposit. Economic Geology, 62, 798–825.

Goldhaber, M. B., Aller, R. C., Cochran, J. K., Rosenfeld, J. K., Martens, C. S., and Berner, R. A. (1977) Sulfate reduction, diffusion, and bioturbation in Long Island Sound sediments: report of the FOAM group. American Journal of Science, 277, 193–237.

Greensmith, J. T., Hatch, F. H., and Rastall, R. H. (1971) Petrology of the Sedimentary Rocks. Thomas Murby and Company, London.

Guidotti, C. V. (1970a) The mineralogy and petrology of the transition from the lower to upper sillimanite zone in the Oquossoc Area, Maine. Journal of Petrology, 11, 277–336.

Guidotti, C. V. (1970b) Metamorphic petrology, mineralogy, and polymetamorphism in a portion of N.W. Maine. In Boone, G. M., Editor, 1970 New England Intercollegiate Geological Conference, 62nd Annual Meeting, Field trip B-1, 1–29.

Guidotti, C. V., Cheney, J. T., and Henry, D. J. (1976) Sulfide-silicate phase relations in metapelites of northwestern Maine. Transactions, American Geophysical Union, 58, 524.

Hewitt, D. A. and Wones, D. R. (1975) Physical properties of some synthetic Fe-Mg-Al trioctahedral biotites. American Mineralogist, 60, 854–862.

Hollister, L. S. and Burruss, R. C. (1976) Phase equilibria in fluid inclusions from the Khtada Lake metamorphic complex. Geochimica et Cosmochimica Acta, 40, 163–175

Kaplan, I. R., Emery, K. O. and Rittenberg, S. C. (1963) The distribution and isotopic abundance of sulfur in recent marine sediments off southern California. Geochimica et Cosmochimica Acta, 27, 297–331.

Kreulen, R. (1980) CO_2-rich fluids during regional metamorphism on Naxos (Greece): carbon isotopes and fluid inclusions. American Journal of Science, 280 745–771.

Leabo, D. A. (1972) Basic Statistics. Richard D. Irwin, Inc., Homewood, Illinois.

Love, L. G. and Amstutz, C. G. (1966) Review of microscopic pyrite. Fortshcritte der Mineralogie, 43, 273–309.

Milner, H. B. (1962) Sedimentary Petrology. The MacMillan Company, New York.

Moore, C. B., Lewis, C. F., Cripe, J., Delles, F. M., and Kelly, W. R. (1972) Total carbon, nitrogen, and sulfur in Apollo 14 lunar samples. Proceedings of the Third Lunar Science Conference, 2, 2051–2058.

Novak, J. M. and Holdaway, M. J. (1981) Metamorphic petrology, mineral equilibria, and polymetamorphism in the Augusta Quadrangle, south-central Maine. American Mineralogist, 66, 51–69.

Oftedahl, C. (1955) On the sulphides of the Alum Shale of Oslo.

Norsk Geologisk Tidsskrift, 35, 117–120.

Osberg, P. H. (1968) Stratigraphy, structural geology, and metamorphism of the Waterville–Vassalboro area, Maine. Maine Geological Survey Bulletin 20.

Osberg, P. H. (1979) Geologic relationships in south-central Maine. In Osberg, P. H. and Skehan, J. W., Editors, The Calendonides in the U.S.A., p. 37–62. Weston Observatory of Boston College, Weston, Massachusetts.

Pettijohn, F. J. (1975) Sedimentary Rocks, Harper and Row, New York.

Popp, R. K. (1977) Wall-rock alteration associated with massive sulfide deposits, Ducktown, Tennessee. Carnegie Institution of Washington Yearbook 76, 603–607.

Popp, R. K., Gilbert, M. C., and Craig, J. R. (1977) Stability of Fe–Mg amphibole with respect to sulfur fugacity. American Mineralogist, 62, 13–30.

Robie, R. A., Bethke, P. M., and Beardsley, K. M. (1967) Selected x-ray crystallographic data, molar volumes, and densities of minerals and related substances. U.S. Geological Survey Bulletin 1248.

Robinson, P. and Tracy, R. J. (1976) Sulfide–silicate–oxide equilibria in sillimanite–K-feldspar pelitic schists, central Massachusetts. Transactions, American Geophysical Union, 58, 524.

Ramdohr, P. (1969) The Ore Minerals and their Intergrowths. Pergamon, Oxford,

Rosenthal, G. (1956) Versuche zur darstellung von markasit, pyrit, und magnetkies aus wässrigen bei zimmertemperatur. Heidelberger Beiträge zur Mineralogie und Petrographie, 5, 146–164.

Rubey, W. W. (1930) Lithologic studies of fine-grained Upper Cretaceous sedimentary rocks of the Black Hills Region. U.S. Geological Survey Professional Paper 165A.

Rumble, D., Ferry, J. M., Hoering, T. C., and Boucot, A. J. (1981) Fluid flow during metamorphism at the Beaver Brook fossil locality, New Hampshire. American Journal of Science, 281, in press.

Ryzhenko, B. N. and Volkov, V. P. (1971) Fugacity coefficients of some gases in a broad range of temperatures and pressures. Geochemistry International, 8, 468–481.

Scott, S. D. (1974) Experimental methods in sulfide synthesis. In Ribbe, P. H., Editor, Sulfide Mineralogy (Mineralogical Society of America Short Course Notes), p. S-1–S-38. Mineralogical Society of America, Chelsea, Michigan.

Shmonov, V. M. and Shmulovich, K. I. (1974) Molar volumes and equation of state of CO_2 at temperatures from 100 to 1000°C and pressures from 2000 to 10,000 bars. Doklady Akademie Nauk SSSR, 217, 206–209.

Skippen, G. B. (1971) Experimental data for reactions in siliceous marbles. Journal of Geology, 79, 457–481.

Smyth, C. H., Jr. (1911) A new locality of pyrrhotite crystals and their pseudomorphs. American Journal of Science, 4th Series, 32, 156–160.

Stull, D. R. and Prophet, H. (1971) JANAF Thermochemical Tables. U.S. Department of Commerce, Washington, D.C.

Sweeney, R. E. and Kaplan, I. R. (1973) Pyrite framboid formation: laboratory synthesis and marine sediments. Economic Geology, 68, 618–634.

Thompson, J. B., Jr. (1972) Oxides and sulfides in regional metamorphism of pelitic schists. Proceedings of the 24th International Geological Congress, Section 10, 27–35.

Toulmin, P. and Barton, P. B., Jr. (1964) A thermodynamic study of pyrite and pyrrhotite. Geochimica et Cosmochimica Acta, 28, 641–671.

Tso, J. L., Gilbert, M. C., and Craig, J. R. (1979) Sulfidation of synthetic biotites. American Mineralogist, 64, 304–316.

Vallentyne, J. R. (1963) Isolation of pyrite spherules from recent sediments. Limnology and Oceanography, 8, 16–30.

Williamson, T. C. and Meyer, G. H. (1969) A pyrite–pyrrhotite isograd in the Waterville area, Maine. Geological Society of America Abstracts with Programs, 1, 237.

Manuscript received, December 5, 1980;
accepted for publication, April 22, 1981.